

Response to the Review Comments

We thank the reviewers for providing insightful comments and helpful suggestions that have substantially improved the manuscript. Below we have included the review comments in italic followed by our responses in blue. In the revised manuscript, we have highlighted those changes accordingly with changes tracked. The line number refers to the ones in the tracked change version manuscript.

Reviewer #1:

The authors present a measurement-based study to report high wintertime HONO concentrations in Nanjing in the YRD area in China, and investigate the contribution of HONO to the atmospheric oxidation capacity in terms of its contribution to the OH formation using a box model. They attribute the high HONO level to the NO₂ heterogeneous reactions on surfaces (particles and ground). Although some results are surprising (for example, photolysis of HONO is the dominant daytime OH source in this area), the methods are overall sound, the paper is well structured and well written in general. The manuscript can be accepted for publication after addressing the following minor issues.

One of the major concerns is that the authors rely considerably on the correlation analysis to reach conclusions, but some of the correlation information may not be valid (a good correlation between two variables does not necessarily mean a cause-and-effect relationship between them). For example, the authors use “The observed similarity between HONO/NO₂ and HONO in diurnal profiles” to “strongly suggests that HONO in the study area was likely originated from NO₂ heterogeneous reactions”. The similarity between HONO/NO₂ and HONO merely suggests that NO₂ does not importantly affect the HONO diurnal variation or NO₂ concentrations are relatively time-invariant (which is indeed the case as shown in Fig. 3). This similarity does not provide any connections between the HONO formation and the NO₂ heterogeneous reaction. Another questionable example is that the authors use “concurrent elevated HONO and PM_{2.5} levels” to “strongly suggest that high HONO may increase the atmospheric oxidation capacity.” Although there is no doubt that high HONO would enhance the atmospheric oxidation capacity and therefore SOA formation, but one could also argue that elevated PM_{2.5} levels lead to elevated HONO due to the heterogeneous reactions and elevated PM_{2.5} levels could be due to emissions. Therefore, the only information of concurrence of elevated HONO and PM_{2.5} levels may not necessarily suggest enhanced oxidation capacity.

Response: We agree with the reviewer that good correlation does not necessarily mean a-cause-and-effect relationship between the two variables. The statement in lines 40-41 has been revised as: “Model simulations indicated that heterogeneous chemistry played an important role in HONO formation”.

Indeed, we cannot quantify how much of the PM_{2.5} was actually from secondary formation. Therefore, we have softened the statement in lines 48-51. It has been revised as "Our study indicated that elevated PM_{2.5} level during the haze events can promote NO₂ to HONO conversion by providing more heterogeneous reaction sites and hence increase the atmospheric oxidation capacity, which may further promote the formation of secondary air pollutants”.

Specific comments:

(1) In Eq. 9, the authors appear to attribute the term of $P_{unknown}$ to the heterogeneous NO_x reactions (including photosensitized and non-photosensitized). In fact, this term should also include HONO emissions and transport (advection). This may partially explain the moderate correlation coefficients (~ 0.5) between this term and $(NO_2).NO_2.RH$ or $J(NO_2).NO_2.S/V.RH$. Although the authors claim that HONO emissions are negligible, the OH production results from two industrial plumes in Fig 6 could also suggest the importance of HONO emissions (besides NO and VOC emissions) to HONO and OH.

Response: We have included the primary emission term in Eqs. 9 and 10 to evaluate its contribution to the total budget of HONO. Both Figs. 9 and 10 have been revised to include the emission term.

$$\frac{d[HONO]}{dt} = (P_{OH+NO} + P_{emission} + P_{unknown}) - (L_{OH+HONO} + L_{photolysis} + L_{deposition}) \quad (9)$$

$$\begin{aligned} P_{unknown} &= \frac{d[HONO]}{dt} + L_{OH+HONO} + L_{photolysis} + L_{deposition} - P_{OH+NO} - P_{emissions} \\ &= \frac{d[HONO]}{dt} + k_{OH+HONO}[OH][HONO] + J_{HONO}[HONO] + \frac{v_{HONO}}{H}[HONO] \\ &\quad - k_{OH+NO}[OH][NO] - \frac{0.003\Delta NO_x}{\Delta t} \end{aligned} \quad (10)$$

Although primary emission of HONO was not substantial but it indeed should not be neglected. In this work, we treated the study area as a standalone "box" and the impact of transport (advection) was not considered. All reactive chemicals affecting HONO were assumed in a steady state and the box model was constrained by the measured species, including VOCs, NO_x , HONO, J-values, and other trace gases. The impact of PM loading on HONO production was also evaluated using the box model in the revised manuscript as suggested by the other reviewer.

(2) In the box model, how is the time variation of the PBL height considered? How it is represented may affect the agreements between observed and simulated HONO concentrations in Fig 10. The authors may also discuss how other limitations or assumptions in the box model affect the simulation results.

Response: The PBL height was based on the remote sounding measurements conducted in Nanjing, a station maintained by the Institute for the Environment (IENV) at the Hong Kong University of Science and Technology (HKUST) (<http://envf.ust.hk/dataview/profile/current/>). The diurnal PBL

profile used here was hourly averaged of all measured data points within December 2015. The uncertainty associated with the model simulations including the limitations in PBL and other input variables were assessed by Monte Carlo analyses. In each Monte Carlo simulation, the input variables of the model, including HONO, O₃, NO, NO₂, CO, SO₂, HCHO, VOCs, reaction rate constants, PBL height, and photolysis frequencies, were independently set to vary within $\pm 10\%$ of the mean value of individual variable with a normal probability distribution (see Lines 222-227). Overall, the Monte Carlo sensitivity analysis show that the model uncertainty of HONO ranged from $\pm 13\%$ to $\pm 38\%$ (see Fig. 10a for details). The sensitivity analysis reinforced the conclusions that the proposed heterogeneous sources can generally capture the observed HONO trend (see Lines 545-549). Also inserted into Fig. 10a are the contributions of primary HONO emission denoted by the brown color. Indeed, primary emission was not trivial. However, primary emission evidently did not contribute significantly to the total HONO budget.

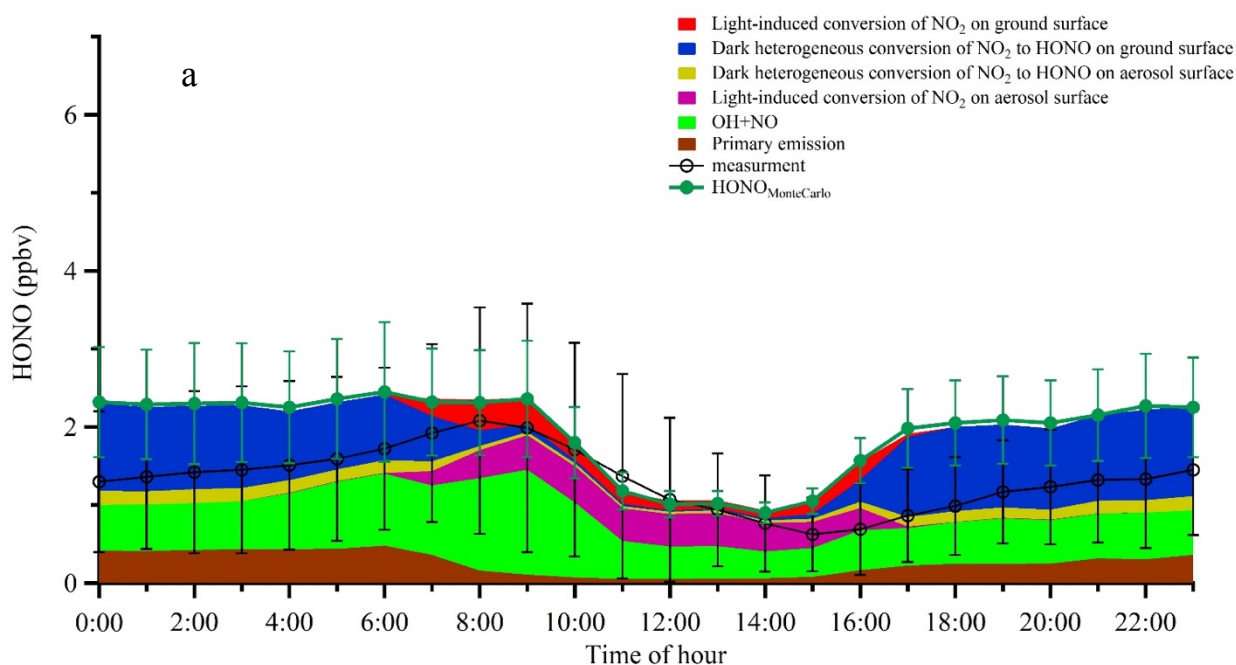


Figure 10a. Averaged diurnal profiles of the measured HONO and the modeled HONO from different sources. Error bars on the black line represent standard deviations of HONO measurements in hourly bins. Error bars on the green markers denote the Monte Carlo analysis results.

Technical corrections:

(1) When several numbers in the same units stand site by site, it is better to just use unit once (e.g., L240, 266, 297-298, 515-517).

Response: Those repeated units have been removed.

(2) In eqn 9, should $\partial[HONO]$ be $d[HONO]$? $\partial t dt$

Response: The Eqs. 9 and 10 all derivatives have been revised into "d/d..." and primary emission is also considered in the equations. Please see response to specific comment #1.

(3) Fig 9, Photolysis should be $L_{\text{photolysis}}$.

Response: Figure 9 legend of photolysis loss has been revised into " $L_{\text{photolysis}}$ ".

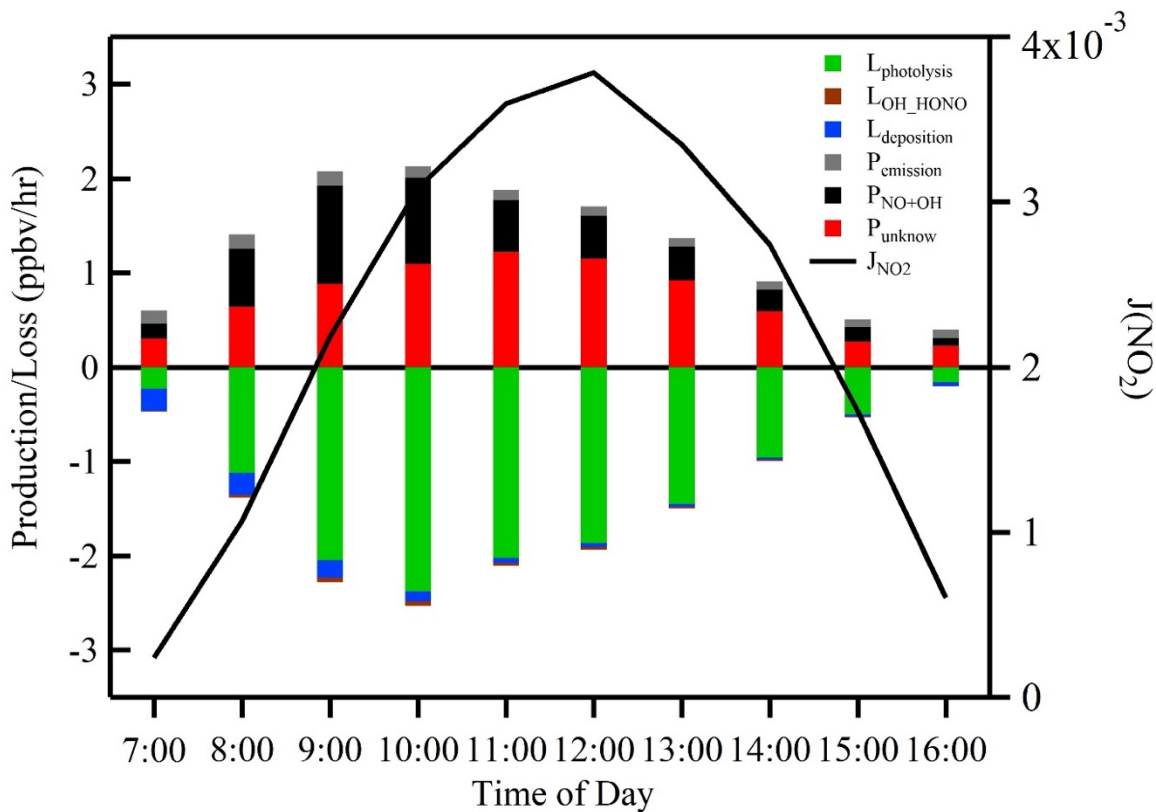


Figure 9. Averaged production and loss rates of daytime HONO and $J(\text{NO}_2)$ during the measurement period. The black line shows the photolysis rate of NO_2 .

Reviewer #2:

This work combines comprehensive field measurements and full box model simulation to investigate the unknown sources of HONO and the contribution to atmospheric oxidation capacity. The results and conclusions highlight the large contribution of HONO to OH radical source and the important role of light-induced enhanced heterogeneous processes in daytime HONO formation. Overall, the manuscript is written with clear logic, fluent language, deep analysis and full discussion. However, there are some major and minor comments which require to be addressed before the manuscript is accepted.

Major comments:

1. *With consideration of the high concentrations of NO (dozens of ppbv) from time to time in the morning from Fig. 2, suggest carefully calculating and assessing the contribution of primary emissions from urban vehicle exhausts to the HONO source.*

Response: As suggested by the reviewer, we have conducted additional model simulations including primary emission as one of the sources. The simulation results are shown in Fig. 10a. Indeed, HONO from primary emissions was not negligible and the model simulations show that it accounts for 11% of the total HONO concentration. We have included the primary emission term in Eqs. (9) and (10). The uncertainty of the model simulation results was assessed by Monte Carlo analysis and the results are displayed in Fig. 10a as green error bars. Overall, the simulation uncertainty varied from $\pm 13\%$ to $\pm 38\%$.

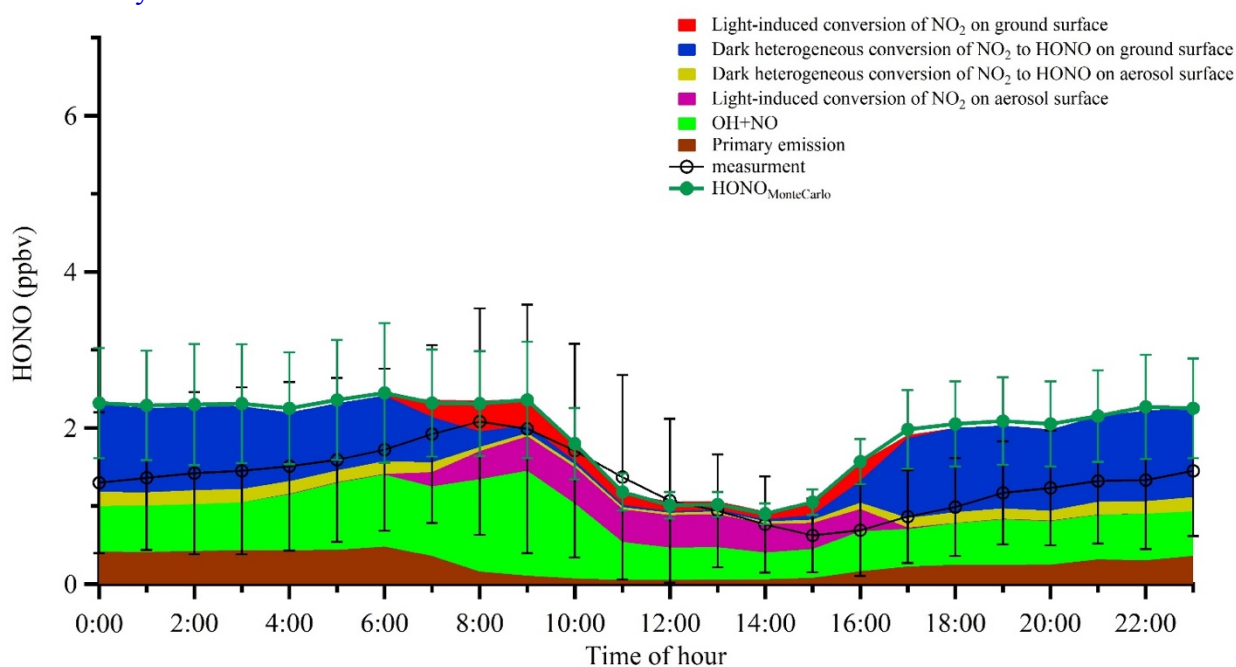


Figure 10a. Averaged diurnal profiles of the measured HONO and the modeled HONO from different sources. Error bars on the black line represent standard deviations of HONO measurements in hourly bins. Error bars on the green markers denote the Monte Carlo analysis results.

2. *Light-induced enhancement of HONO formation on aerosol surfaces was found by the authors, particularly within industrial plumes. So, what photosensitized aerosol components were*

responsible for the photo-catalyzed processes? Aerosol composition data or additional discussions are required to elaborate this issue.

Response: We agree with the reviewer it would be ideal to have aerosol chemical composition information to support our conclusion. Unfortunately, aerosol chemical composition was not measured during this work. However, since the photo-enhanced HONO formation only proceeds on aerosol surfaces, aerosol chemical composition may not be able to directly reflect aerosol surface chemical property. The detailed mechanisms underlying the light-induced HONO formation on aerosol surfaces are still under active research. It is believed to be highly dependent on the surface properties. For example, the conversion rates on soot surface (Han et al., 2017) and organic surface (Stemmler et al., 2006) can vary substantially. In addition, laboratory studies have found that this mechanism is not catalytic by the surface in nature and the rate of which may vary with the availability and aging state of the surface reaction sites. Therefore, aerosol chemical composition alone may not be sufficient to deduce the actual HONO formation mechanism. Currently, in atmospheric chemistry models the light-induced HONO formation process was only treated as a bulk reaction on the aerosol surface with a substantial faster surface uptake coefficient of NO₂ (Huang et al., 2017; Li et al., 2018; Wang et al., 2017). We have added the following statement in the manuscript (Lines 482-489) to further elaborate this issue.

“Since aerosol chemical composition was not measured in this work, we cannot demonstrate any possible direct connection between aerosol composition and the photo-enhanced HONO formation on aerosol surfaces. Nevertheless, the actual mechanism underlying the photo-enhanced HONO formation on aerosol surface need further investigation. It has been found that photo-sensitized NO₂ conversion rate coefficient on different surfaces can vary substantially (Han et al., 2017; Stemmler et al., 2006). Furthermore, studies have shown that this type of surface reaction is not catalytic in nature and the surface reaction rate may vary with the availability and aging state of the surface reaction sites (Stemmler et al., 2006). Therefore, aerosol chemical composition alone may not be sufficient to reveal the actual HONO formation processes.”

3. The accurate simulation by using one-dimension box model requires stable meteorological conditions. In this study, how to select the simulation periods and what are the criteria?

Response: The model we used in this study is a box model or 0-dimensional (not one-dimensional) model which does not require stable meteorological conditions. The box model was constrained by the observed meteorological conditions (temperature, pressure, humidity, photolysis frequencies) and chemical species. We agree with the reviewer that meteorological conditions can significantly affect the air pollution level at an observation site through transport or convection. A 3-D model would be ideal to investigate both physical and chemical processes that could affect the HONO chemistry. However, the accuracy of a 3-D model would rely heavily on the accuracy of emission inventory and meteorological field used in the model, which were basically unavailable for the study area. In addition, to accomplish a 3-D modeling work was far beyond the scope of this work.

The objective of this work was to investigate the impacts of HONO chemistry on the local atmospheric oxidative capacity through a comprehensive field campaign at one supersite. Since no transport and vertical mixing were considered here, a 0-D box model should be sufficient to do the job. Especially the observation period was during winter time, when wind field was relatively

weak with an average wind speed of 1.7 m s^{-1} and the solar radiation was less intense, leading to weaker vertical mixing. Therefore, the winter weather condition would make the observation site prone to local air pollution accumulation, which would justify the usage of a simple 0-D box model.

Minor comments:

1. Line 37–39, point out the detailed period of time.

Response: These numbers are campaign averaged results. The exact campaign period “from 1 to 31 December 2015” has been inserted into the sentence in Line 32 after “China”. A phrase “during the campaign period” has been inserted in Line 37 after “The results show that...”.

2. Line 172, how about the zero calibration or background detection for the HONO measurement? With zero air or using other method?

Response: As described in Section 2.1 and illustrated in Fig. 1, a configuration of two samplers in serial is used with the first sampler to measure the total signal and the second sampler to measure background signal. The difference between the two samplers is the net HONO signal. The background signal is usually only a few percent of the total signal. We have added the following few sentences (Lines 165-168):

“Two coil samplers in serial were used to measure total signals in the first sampler and the background in the second sampler. The difference between the two samplers is the net HONO signal. The background signal is usually only a few percent of the total signal.”

The instrument calibration was carried out by injecting standard NaNO_2 solution into the instrument right after the sampling coil. During the campaign period, the instrument was calibrated once every four days and the HONO data in between calibrations were adjusted with the calibration factors accordingly.

We have inserted the following statement into the supporting information to further explain the HONO instrument operation: (Lines 184-186)

“The instrument calibration was carried out once every four days by injecting standard sodium nitrite (NaNO_2) solution into the instrument right after the sampling coil.

3. Line 206-207, describe the potential uncertainty aroused by the limited VOC species used in the box model.

Response: In this work, a GC-FID instrument was used to measure 60 VOCs, including most alkanes, alkenes, and aromatics. Although oxygenated VOCs (OVOCs) were missing except formaldehyde and a few other carbonyls detected by a DHPL method, we constrained the box model with measured VOCs. The model results show that OVOCs only accounted for a very small portion of the total VOCs in this industrial area. Moreover, OVOCs even contributed much less to the total VOC OH reactivity. Therefore, we believe the missing OVOC (except carbonyl compounds) would not significantly affect our model simulation results. We have inserted the following statement into the manuscript (Lines 222-227):

“Although the oxygenated VOCs (OVOCs) other than formaldehyde and some other carbonyls (by the DNPH method) were not measured in this study, they were simulated in the box model that

was constrained to measured VOC. Our results indicated that OVOCs only accounted for a small portion of the total VOCs in this industrial area and even contributed much less to the total VOC OH reactivity. Therefore, the limited VOCs detected in this work would not significantly affect the following model simulation results.”

4. Line 214, “VOC” can be “VOCs”.

Response: It has been changed to VOCs.

5. Line 235, 238, 239, suggest adding a word such as “averaging” before the “maxiuma” and “minimum”.

Response: We have inserted “daily averaged” before “maxima” and “minimum”.

6. Line 241–243, the “similarity between the diurnal profile of HONO/NO₂ ratio and that of HONO” cannot suggest that HONO was likely originated from NO₂ heterogeneous reactions. Unchanged NO₂ concentration also led to similar trends between HONO/NO₂ ratio and HONO concentration. Similar trends between HONO/NO₂ ratio and S/V ratio could be an evidence for heterogeneous formation on aerosol surfaces.

Response: We agree with the reviewer and the statement has been removed to avoid misleading.

7. Line 295, state the possible uncertainty or influence on the model simulation results due to the assumption of constant H₂O₂ concentration of 3 ppbv. A linear or non-linear estimation of H₂O₂ concentration from other pollutants or parameters is better than a constant value.

Response: The H₂O₂ level is unknown in the study area and H₂O₂ measurements were seldom conducted in China. However, H₂O₂ is much less photo-sensitive than other major OH precursors, such as O₃, HCHO and HONO. Model simulation tests with doubled H₂O₂ concentration can only cause a few more percent increase in OH production from H₂O₂ photolysis, which was significantly lower than the model uncertainty estimated by the Monte Carlo analysis. Therefore, we believe H₂O₂ would not contribute significantly to the total OH budget estimation. Moreover, estimation of H₂O₂ as a function of other parameters cannot be supported by our other measurements that may also introduce other much larger uncertainties.

8. Line 300, point out the detailed period of time, e.g., 7:00-16:00 local time.

Response: We have modified the sentence in Line 321

“As shown in Fig. 5, the contribution of HONO photolysis to OH production during 7:00-16:00 local time varied from 23.6% to 63.3% with a mean value of 44.8%.”

9. Line 334–336, are there PM_{2.5} composition data to support that most of the PM_{2.5} components came from secondary formation during the two industrial plume events and the enhancement of secondary aerosol components simultaneously occurred with elevated HONO photolysis rate? If

there is no enough evidence, suggest removing the deduction that “high levels of HONO promote the formation of PM_{2.5}” in the main text, Abstract, and Highlights.

Response: PM_{2.5} composition was not measured in this work. The statement in the abstract has been removed. The sentence in Line 356 has been revised as:

“Although ambient OH concentrations during these events may not be high (see Fig. 4a), the high levels of HONO can boost active photochemical oxidation and thus promote the formation of other secondary air pollutants.”

Highlight#3 has been revised as:

“High loading of PM_{2.5} provided additional reaction surfaces for HONO formation.”

10. Line 342, the HONO emission ratio was expressed as HONO/NO_x ratio, right?

Response: Yes, the HONO emission ratio was expressed as HONO/NO_x ratio. It has been revised accordingly.

11. Line 350– 351, with consideration of the high concentration of NO particularly in the morning (see Fig. 3), the influence of traffic source possibly cannot be ignored. Suggest carefully evaluating the influence from traffic source.

Response: As suggested by both reviewers we have included the primary HONO emission into the model simulation to assess the impacts of primary emission more accurately. We have revised Section 3.5.1 :

“Previous studies have demonstrated that HONO can be emitted directly from vehicle exhaust (Kirchstetter et al., 1996; Kurtenbach et al., 2001). However, the NO/NO_x ratio measured in this work was relatively low, with an average of 0.25 ± 0.06 , much less than that of freshly emitted exhausts (> 0.9) obtained from tunnel experiments (Kurtenbach et al., 2001), indicating that the air masses sampled in this work had been considerably aged and mixed with other air masses, and hence primary HONO from direct emission (if there was any) had been diluted substantially (less than a few per cents) before reaching the observation site. In addition, our sampling site is located nearby the industrial zone, and the high concentration of NO_x was mainly originated from the industrial activities, so the influence of traffic source on HONO was expected to be small. To further evaluate the potential impact of primary emissions on HONO concentration, we have incorporated the contribution of primary HONO emission into the MCM box model. The HONO emission ratios, i.e., HONO/NO_x, was taken as 0.3% (Kirchstetter et al., 1996), representing a gasoline-fueled vehicle fleet, which was very typically encountered in the study area. On average, the primary emissions from vehicle exhaust can only account for 11% of the total HONO concentration, indicating secondary mechanisms still dominated HONO level in the study area, which will be further analyzed in the following sections.”

In addition, the simulation results are included in the new Fig. 10a. Please see response to the specific comment #2 of reviewer #1 for details. Indeed, although primary HONO emission was not substantial, it should not be neglected.

12. Line 357, as to “the two different time points”, how were the time periods selected? Based on what criteria?

Response: There is no commonly-accepted criteria for time period selection that is used to calculate the NO₂ to HONO conversion ratio. In summary, we searched through the HONO and NO₂ timeseries for periods when both of them increased monotonically with a correlation coefficient higher than 0.8. The following sentence has been inserted into Line 390-392:

“The time periods used to calculate HONO/NO₂ conversion ratio were selected when both HONO and NO₂ increased monotonically with a correlation coefficient higher than 0.8.”

13. Line 374, as to “for several individual days”, which days? What are the criteria for the selection?

Response: The individual days referred to days when industrial plumes were encountered at the site, i.e., the 7, 21, and 22 of December. The data on these days have been used to generate Fig. 10b. In addition, we have conducted additional model sensitivity study with respect to aerosol surface area. Therefore, we have removed these correlation analysis results from the manuscript.

14. Line 397, “timely” can be temporal.

Response: “Timely” has been changed to “temporal”.

15. Line 413, carefully evaluate the HONO emission from traffic sources, due to sometimes NO concentration was very high, particularly in the morning (see Fig. 3).

Response: The primary HONO emission has been included in the daytime HONO budget evaluation. We have revised the sentence as: “The impact of HONO direct emissions was relatively small at daytime.” (Line 456)

16. Line 498–500, were there aerosol composition data to show the fractions of secondary components and primary components during the industrial plume events? Were there high levels of photosensitized components such as metals, black carbons, and brown carbons?

Response: Aerosol chemical composition was not measured during this work. We have downplayed the discussions on the correlations between HONO and PM_{2.5}. Please see responses to major comments #2 and minor comments #9.

17. Line 524–525 and the subsequent paragraph, was the enhanced HONO formation during daytime was dominated by humid heterogeneous reactions, or photosensitized reactions, or together?

Response: New model simulation including HONO primary emission showed that the enhanced HONO formation during daytime was mainly due to photosensitized reactions on both aerosol surface (28.2%) and ground surface (17.8%). The heterogeneous mechanism only accounted for 2.2% from aerosol surface and 7.9% from ground surface. The sentence in Lines 583-587:

“The model suggests that higher daytime levels of HONO were mainly produced by the light-induced conversion of NO₂ on aerosol surfaces (28.2%) and ground surfaces (17.8%) (except early morning). While the heterogeneous HONO production on ground surface dominated nocturnal HONO sources, heterogeneous reactions on various surfaces only contributed a small portion of total HONO at daytime (2.2% on aerosol surface and 7.9% on ground surface).”

Reviewer #3:

1) This manuscript reports the results of a field campaign in Nanjing, a megacity within the Yangtze River Delta (YRD) region, during December, 2015. HONO and related species were simultaneously measured. High levels of (especially daytime) HONO were reported and were most likely due to heterogeneous reactions involving NO₂. YRD is one of the most developed and also polluted regions of China. Atmospheric oxidation capacity (mostly determined by the OH radical) is the fundamental driving force that is responsible for the fast formation of secondary air pollutants such as O₃ and PM. Although observations of high levels of HONO are not surprising in China, such a comprehensive field campaign like this study is still of practical importance to fully understand the role of HONO chemistry in this region. Especially, the budget of OH radical in the YRD region shall be extensively assessed. The subject of this study is within the scope of ACP. Overall, the experimental methodology is generally sound and the measurements were properly conducted. The manuscript is fairly well written and the logic is clear to follow. One of my major concerns is that the authors claim that primary emission did not contribute significantly to the observed HONO. But I would suggest the authors to further evaluate the significance of primary emission using the box model, which should be able to give a more reliable and quantitative assessment of primary emitted HONO.

Response: We appreciate the helpful suggestion from the reviewer and we have conducted additional model simulations including primary emission as one of the sources. The emission ratios of HONO with respect to NO_x (HONO/NO_x) was taken from the results obtained from tunnel measurements of Kirchstetter et al. (1996), i.e., 0.3%, which represented a gasoline powered vehicle fleet, which was typically encountered in the study area. Also, it should be noted that some the measured HONO may be originated from heterogeneous reactions on various surfaces during the tunnel experiments. Therefore, the estimated HONO emissions should be taken as an upper limit. The simulation results are shown in Fig. 10a. Indeed, although the contribution from primary HONO emission was relatively small, it should not be neglected.

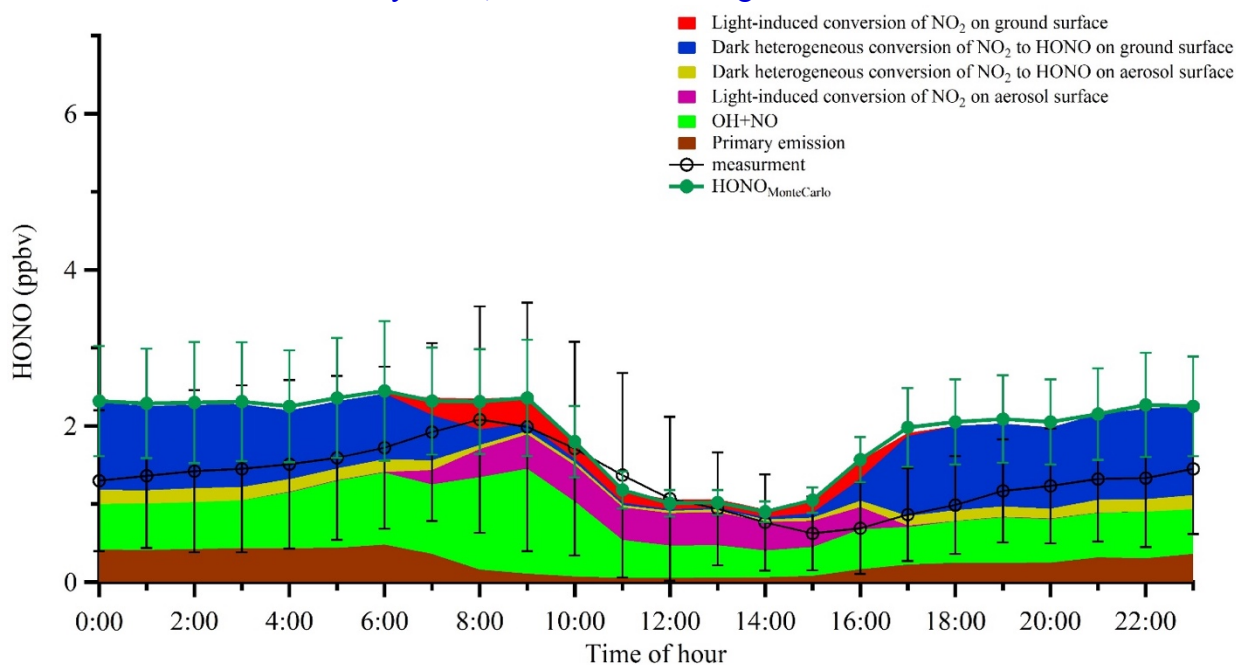


Figure 10a. Averaged diurnal profiles of the measured HONO and the modeled HONO from different sources. Error bars on the black line represent standard deviations of HONO measurements in hourly bins. Error bars on the green markers denote the Monte Carlo analysis results.

2) Also, I would suggest the authors to weaken the role of correlation analysis (Section 3.5.5) and rely more on the model simulation results. The good correlation between aerosol surface density and HONO does not necessarily mean that HONO is produced on aerosol surfaces. A model sensitivity study would be a better way to verify if high loading of PM was playing an important role in HONO formation by promoting heterogeneous reactions.

Response: Yes, we agree with the reviewer that a simple correlation analysis is not sufficient to establish the connection between HONO formation and aerosol surface area. We have conducted extra model sensitivity study to verify the impacts of aerosol surface on HONO production. By decreasing and increasing the aerosol surface area density by a factor of 2, respectively. The results showed that the contribution from heterogeneous photosensitized conversion of NO₂ on aerosol surfaces would correspondingly vary from 18% to 40% of the total HONO budget. Therefore, we believe aerosol surface played an important role in HONO photosensitized formation in the study area. A statement has been inserted into Lines 545-549:

“In addition, we have performed a model sensitivity study with respect to aerosol surface density by varying S/V from 50% to 200% of the average value. The results showed that the contribution from heterogeneous photosensitized conversion of NO₂ on aerosol surfaces would correspondingly vary from 18% to 40% of the total HONO budget, demonstrating that aerosol surface chemistry played an important role during HONO formation in the study area.”

Technical comments:

- 1) L103: “because”
- 2) L273: “heterogeneous”
- 3) L329: “the origins of these...”
- 4) L368: “appears”

Response: The above typos have been corrected and the manuscript has been revised accordingly.

References:

Han, C., Liu, Y., and He, H.: Heterogeneous reaction of NO₂ with soot at different relative humidity., *Environ. Sci. Pollut. Res.*, 24, 21248–21255, 10.1007/s11356-017-9766-y, 2017.

Huang, R.-J., Yang, L., Cao, J., Wang, Q., Tie, X., Ho, K.-F., Shen, Z., Zhang, R., Li, G., Zhu, C., Zhang, N., Dai, W., Zhou, J., Liu, S., Chen, Y., Chen, J., and O'Dowd, C. D.: Concentration and sources of atmospheric nitrous acid (HONO) at an urban site in Western China, *Sci. Total Environ.*, 593-594, 165-172, <https://doi.org/10.1016/j.scitotenv.2017.02.166>, 2017.

Kirchstetter, T. W., Harley, A. R., and Littlejohn, D.: Measurement of nitrous acid in motor vehicle exhaust, *Environ. Sci. Technol.*, 30, 2843–2849, 10.1021/es960135y, 1996.

Kurtenbach, R., Becker, K. H., Gomes, J. A. G., Kleffmann, J., Lörzer, J. C., Spittler, M., Wiesen, P., Ackermann, R., Geyer, A., and Platt, U.: Investigations of emissions and heterogeneous formation of HONO in a road traffic tunnel, *Atmos. Environ.*, 35, 3385-3394, [https://doi.org/10.1016/S1352-2310\(01\)00138-8](https://doi.org/10.1016/S1352-2310(01)00138-8), 2001.

Li, D., Xue, L., Wen, L., Wang, X., Chen, T., Mellouki, A., Chen, J., and Wang, W.: Characteristics and sources of nitrous acid in an urban atmosphere of northern China: Results from 1-yr continuous observations, *Atmos. Environ.*, 182, 296-306, <https://doi.org/10.1016/j.atmosenv.2018.03.033>, 2018.

Ren, X., Gao, H., Zhou, X., Crouse, J. D., Wennberg, P. O., Browne, E. C., LaFranchi, B. W., Cohen, R. C., McKay, M., Goldstein, A. H., and Mao, J.: Measurement of atmospheric nitrous acid at Blodgett Forest during BEARPEX2007, *Atmos. Chem. Phys.*, 10, 6283-6294, 10.5194/acp-10-6283-2010, 2010.

Stemmler, K., Ammann, M., Donders, C., Kleffmann, J., and George, C.: Photosensitized reduction of nitrogen dioxide on humic acid as a source of nitrous acid, *Nature*, 440, 195-198, 10.1038/nature04603, 2006.

Wang, J., Zhang, X., Guo, J., Wang, Z., and Zhang, M.: Observation of nitrous acid (HONO) in Beijing, China: Seasonal variation, nocturnal formation and daytime budget, *Sci. Total Environ.*, 587-588, 350-359, <https://doi.org/10.1016/j.scitotenv.2017.02.159>, 2017.

1 **Contribution of HONO to the atmospheric oxidation capacity in an industrial zone**
2 **in the Yangtze River Delta region of China**

3 Jun Zheng^{1*}, Xiaowen Shi¹, Yan Ma^{1,2}, Xinrong Ren^{3,4,5}, Halim Jabbour¹, Yiwei Diao^{1,6}, Weiwei Wang⁶, Yifeng
4 Ge¹, Yuchan Zhang¹, and Wenhui Zhu¹

5 ¹Collaborative Innovation Center of Atmospheric Environment and Equipment Technology, Nanjing University
6 of Information Science & Technology, Nanjing 210044, China

7 ²NUIST Reading Academy, Nanjing University of Information Science & Technology, Nanjing 210044, China

8 ³Air Resources Laboratory, National Oceanic and Atmospheric Administration, College Park, Maryland, USA

9 ⁴Department of Atmospheric and Oceanic Science, University of Maryland, College Park, Maryland, USA

10 ⁵Cooperative Institute for Satellite Earth System Studies, University of Maryland, College Park, Maryland, USA

11 ⁶Key Laboratory for Aerosol-Cloud-Precipitation of China Meteorological Administration, Department of
12 Atmospheric Physics, Nanjing University of Information Science and Technology, Nanjing 210044, China

13

14 *Correspondence to: Dr. Jun Zheng (zheng.jun@nuist.edu.cn)*

15 *Address: School of Environmental Science and Engineering, Nanjing University of Information*

16 *Science & Technology, Nanjing 210044, China*

17 *Tel.: +86-18251919852*

18 *Fax: +86-25-58731090*

19

20 **Key points:**

- 21 • High levels of HONO, with an average of 1.32 ± 0.92 ppbv, were observed near one of the largest industrial
22 zones in the YRD region of China.
- 23 • HONO photolysis and alkene ozonolyses contributed the most of OH production and hence the atmospheric
24 oxidation capacity.
- 25 • High loading of PM_{2.5} [provided additional reaction surfaces for HONO formation.](#)
- 26 • Heterogeneous formation mechanisms were the most important daytime HONO sources and were further
27 enhanced by sunlight.

28 **Abstract**

29 A suite of instruments were deployed to simultaneously measure nitrous acid (HONO), nitrogen oxides (NO_x
30 = NO + NO₂), carbon monoxide (CO), ozone (O₃), volatile organic compounds (VOCs, including formaldehyde
31 (HCHO)) and meteorological parameters near a typical industrial zone in Nanjing of the Yangtze River Delta region,
32 China [from 1 to 31 December 2015](#). High levels of HONO were detected using a wet chemistry-based method.
33 HONO ranged from 0.03-7.04 ppbv with an average of 1.32 ± 0.92 ppbv. Elevated daytime HONO was frequently
34 observed with a minimum of several hundreds of pptv on average, which cannot be explained by the homogeneous
35 OH + NO reaction (P_{OH+NO}) [and primary emission \(P_{emission}\)](#), especially during periods with high loadings of
36 particulate matters (PM_{2.5}). The HONO chemistry and its impact on atmospheric oxidation capacity in the study
37 area were further investigated using a MCM-box model. The results show that [during the campaign period](#) the
38 average hydroxyl radical (OH) production rate was dominated by the photolysis of HONO (7.13×10^6 molecules
39 cm⁻³ s⁻¹), followed by ozonolysis of alkenes (3.94×10^6 molecules cm⁻³ s⁻¹), photolysis of O₃ (2.46×10^6 molecules
40 cm⁻³ s⁻¹) and photolysis of HCHO (1.60×10^6 molecules cm⁻³ s⁻¹), especially within the plumes originated from the
41 industrial zone. [Model simulations indicated that heterogeneous chemistry played an important role in HONO](#)

42 formation. The average nighttime NO₂ to HONO conversion rate was determined to be ~0.8% hr⁻¹. Good correlation
43 between nocturnal HONO/NO₂ and the products of particle surface area density (S/V) and relative humidity (RH),
44 S/V·RH, supports the heterogeneous NO₂/H₂O reaction mechanism. The other HONO source, designated as
45 P_{unknown}, was about twice as much as P_{OH+NO} on average and displayed a diurnal profile with an evidently photo-
46 enhanced feature, i.e., photosensitized reactions of NO₂ may be an important daytime HONO source. Nevertheless,
47 our results suggest that daytime HONO formation was mostly due to the light-induced conversion of NO₂ on aerosol
48 surfaces but heterogeneous NO₂ reactions on ground surface dominated nocturnal HONO production. Our study
49 indicated that elevated PM_{2.5} level during the haze events can promote NO₂ to HONO conversion by providing
50 more heterogeneous reaction sites and hence increase the atmospheric oxidation capacity, which may further
51 promote the formation of secondary air pollutants.

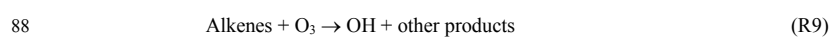
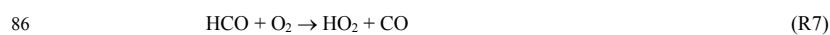
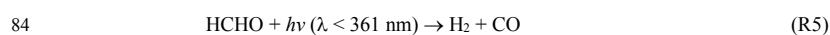
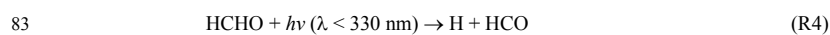
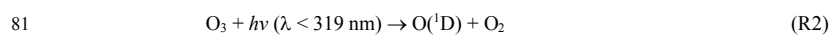
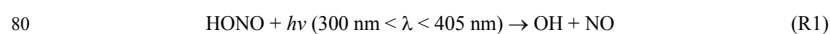
Deleted: The observed similarity between HONO/NO₂ and HONO in diurnal profiles strongly suggests that HONO in the study area was likely originated from NO₂ heterogeneous reactions.

52 1 introduction

53 Nitrous acid (HONO) plays an important role in tropospheric photochemistry because its fast photolysis
54 contributes to the formation of hydroxyl (OH) radical, which is an essential atmospheric oxidant that initiates the
55 oxidation of volatile organic compounds (VOC) to form organic peroxy radicals (RO₂) and hydroperoxyl radical
56 (HO₂). In the presence of nitrogen oxides (NO_x = NO + NO₂), these free radicals are the fundamental driving force
57 of photochemical reaction cycles that lead to the formation of ground-level ozone (O₃) and secondary organic
58 aerosols (SOA) (Finlayson-Pitts and Pitts, 1999; Xue et al., 2016). Besides HONO photolysis (R1), the major
59 known OH radical initiation sources include photolysis of O₃ (R2 and R3) and formaldehyde (HCHO) (R4 to R8),
60 and ozonolysis of alkenes (R9) (Finlayson-Pitts and Pitts, 1999). Nevertheless, many field studies have
61 demonstrated that HONO may strongly affect atmospheric oxidation capacity in various environments (Bernard et
62 al., 2016; Elshorbany et al., 2009; Elshorbany et al., 2010; Zhou et al., 2002). In early studies, HONO was believed
63 to be only important as NO_x reservoir during nighttime, when HONO can accumulate in the atmosphere and give

Deleted: Concurrent elevated HONO and PM_{2.5} levels strongly indicate that high HONO may increase the atmospheric oxidation capacity and further promote the formation of secondary aerosols, which may in turn synergistically boost NO₂/HONO conversion by providing more heterogeneous reaction sites.

74 a boost of photochemistry in the following early morning (Platt et al., 1980). However, recent field studies have
75 demonstrated that high concentrations of HONO are often present in the relatively polluted urban areas during the
76 day. Because of high levels of HONO, the photolysis of HONO becomes an important OH source not only in the
77 early morning but also throughout the day and can contribute up to 30-90% of OH radical during daytime (Acker
78 et al., 2006; Hendrick et al., 2014; Kleffmann et al., 2005; Neftel et al., 1996; Spataro et al., 2013; Su et al., 2008;
79 Zhou et al., 2002).



89 Despite the significance of HONO in daytime photochemistry, the sources and formation mechanisms of
90 HONO, especially during daytime, are still uncertain. Traditionally, the reaction between NO and OH was thought
91 to be the most important homogeneous source for HONO (Perner and Platt, 1979):



93 However, reaction R10 alone cannot sustain the high HONO level observed during daytime in many studies, in
94 which the observed HONO levels were often an order of magnitude greater than the modeled HONO with only
95 homogeneous HONO source (R10) included in the model (Ren et al., 2010; Tang et al., 2015). Nevertheless, higher
96 than expected OH observed in several studies (Hofzumahaus et al., 2009) may explain partially observed higher

97 than model predicted HONO levels. It has been suggested that HONO may be emitted directly by incomplete
98 combustion processes, such as vehicle exhaust (Kirchstetter et al., 1996; Kurtenbach et al., 2001; Liang et al., 2017;
99 Nakashima and Kajii, 2017; Trinh et al., 2017; Xu et al., 2015) and biomass burning (Müller et al., 2016; Neuman
100 et al., 2016; Nie et al., 2015; Rondon and Sanhueza, 1989). However, such strong but sporadic point sources could
101 not account for the widely observed daytime HONO in the polluted areas (Elshorbany et al., 2012; Wang et al.,
102 2017). Recently, many other HONO formation pathways have been proposed. Su et al. (2011) pointed out that
103 HONO can be released from soil nitrite, which was formed through biological nitrification and denitrification
104 processes. Recent studies demonstrated that the pH and organic content of soil could influence the HONO emission
105 rate (Scharko et al., 2017; Sörgel et al., 2015). In addition, vertical profiles of HONO measurements indicated that
106 HONO was very likely originated from the ground surface (Kleffmann et al., 2003; VandenBoer et al., 2013; Wong
107 et al., 2011; Wong et al., 2013). However, the presence of in-situ HONO sources in the air masses aloft cannot be
108 ruled out (Wong et al., 2013; Zhang et al., 2009).

109 Several heterogeneous processes have been drawn substantial attention and are proposed as the major HONO
110 sources, including: (1) heterogeneous conversion of NO₂ on wet surface (Finlayson-Pitts et al., 2003), which could
111 be an important nocturnal HONO source; (2) NO₂ heterogeneous reaction with fresh soot particles (Ammann et al.,
112 1998; Gerecke et al., 1998; Han et al., 2017a; Monge et al., 2010) and semi-volatile organic compound emitted
113 from diesel exhausts (George et al., 2005; Gutzwiller et al., 2002), which could be an important process **because** it
114 is 1 to 2 orders of magnitude faster than the typically proposed heterogeneous reaction of 2NO₂ + H₂O; (3)
115 photosensitized reaction of NO₂ on surfaces of mineral dust (Ndour et al., 2008), humic acid (Han et al., 2017b;
116 Wall and Harris, 2016), and ground surface (i.e., certain reactions such as NO₂ + humic acids on ground surfaces)
117 (Wong et al., 2012), which has been considered as an important daytime HONO source (Lee et al., 2016); (4)
118 photolysis of adsorbed nitric acid (HNO₃) and nitrate (NO₃⁻) (Ye et al., 2016; Ye et al., 2017; Zhou et al., 2002;
119 Zhou et al., 2003; Zhou et al., 2011; Ziemba et al., 2010); (5) VOC-mediated conversion of HNO₃ into HONO

120 (Gall et al., 2016).

121 Since the first atmospheric HONO measurement by Nash (1974) and the first use of long path differential UV
122 absorption technique (LP-DOAS) to measure atmospheric HONO (Perner and Platt, 1979), various measurement
123 techniques for HONO have been developed, such as spectroscopic techniques, wet chemistry-based techniques,
124 and chemical ionization mass spectrometry (CIMS). Besides DOAS technique, other spectroscopic techniques such
125 as the cavity ring-down spectroscopy (Rairoux et al., 2002), the incoherent broadband cavity-enhanced absorption
126 spectroscopy (IBBCEAS) (Gherman et al., 2008), and the cavity-enhanced absorption spectrometer (CEAS)
127 (Scharko et al., 2017) were applied in the HONO measurements. Wet chemistry techniques have the advantages of
128 higher sensitivity and lower detection limit, including long path absorption photometer (LOPAP) (Heland et al.,
129 2001; Kleffmann et al., 2003; Kleffmann et al., 2005; Kleffmann et al., 2006; Kleffmann and Wiesen, 2008; Vecera
130 and Dasgupta, 1991), AIM-IC analysis system and wet-rotating-denuder (WRD) method (Makkonen et al., 2012).
131 Very recently, CIMS techniques have been developed for fast on-line HONO measurements (Bernard et al., 2016;
132 Pinto et al., 2014; Ren et al., 2010).

133 Yangtze River Delta (YRD) region is the largest industrial zone in China and is experiencing ever increasing
134 air pollution events, characterized with high ozone (O_3) and fine particulate matters ($PM_{2.5}$) concentrations (Ding
135 et al., 2013). Despite of the great efforts in reducing sulfur dioxide (SO_2) and NO_x emissions from industrial
136 activities, high level of NO_x along with ammonia/amines have been observed near an industrial park (Zheng et al.,
137 2015b). In addition, high levels of HCHO have been frequently observed near industrial zones in China (Ma et al.,
138 2016; Wang et al., 2015b), providing an extra radical source. HONO concentrations calculated using a
139 photostationary state (PSS) approach that included homogeneous sources were found much less HONO than the
140 measured values during daytime (Kleffmann et al., 2005; Michoud et al., 2014). Lee et al. (2016) conducted a
141 detailed analysis of HONO budget and proposed that the missing daytime HONO source was related to NO_2 and
142 sunlight. A four-season measurement campaign was carried out in an urban site of Beijing and the results showed

143 monthly averaged HONO concentrations between 1.05 and 2.27 ppbv with pronounced seasonal profile (Wang et
144 al., 2017). In a recent study, Nie et al. (2015) revealed the influence of biomass burning on HONO formation at a
145 suburban site of Nanjing and demonstrated that the contribution of heterogeneous conversion of NO₂ to HONO
146 formation. However, so far, no comprehensive study on the oxidizing capability, i.e., the major contributors of OH
147 radicals, has ever been conducted in the industrial zone of YRD region.

148 In this work, we have performed HONO measurements using a custom-built wet chemistry-based method at
149 an industrial site in December 2015 in Nanjing, China. In addition, HCHO, O₃, photolysis frequencies, and other
150 trace gases and meteorological parameters were also measured. The contributions of HONO along with other OH
151 sources to OH budget were investigated using a box model based on Master Chemical Mechanism (MCM). The
152 mechanisms of possible daytime HONO formation and the consequent impacts on air pollutants formation were
153 explored.

154

155 **2 Experimental and Model Description**

156 **2.1 HONO Measurement**

157 The field measurements were carried out from 1 to 31 December 2015 on the campus of Nanjing University
158 of Information Science and Technology (NUIST) in Nanjing, China. More details about the observation site have
159 been provided in our previous work (Ma et al., 2016; Zheng et al., 2015b). Briefly, the site is located to the west of
160 clusters of steel mills and petrochemical refinery facilities and is about 15 km to the north of the downtown Nanjing.
161 All instruments were placed inside an air-conditioned trailer. In this study, a custom-built wet chemistry-based
162 HONO instrument was utilized for HONO measurements, which was originally developed by Ren et al. (2010).
163 Figure 1 is the schematics of the HONO instrument, consisting of two sample collection glass coils connected

164 successively, a 10-port injection valve (Valco Instruments Co. Inc.), a 1-m long liquid waveguide capillary cell
165 (LWCC, World Precision Instruments), and a mini spectrometer (Ocean optics, USB4000). Two coil samplers in
166 serial were used to measure total signals in the first sampler and the background in the second sampler. The
167 difference between the two samplers is the net HONO signal. The background signal is usually only a few percent
168 of the total signal.

169 To minimize the sampling artifacts, the sampling coils were set up about 3.5 m above the ground (1.5 m above
170 the trailer rooftop) and no inlet was used. Ambient air was pulled through the coils by a vacuum pump at 1 L min⁻¹,
171 which was controlled by a mass flow controller (MKS, model M100B). In the first coil, HONO along with some
172 interfering species in the air sample were separated from the gas phase and transformed into nitrite solution by a
173 1.0 mmol L⁻¹ phosphate buffer scrubbing solution. Potential interfering species (e.g., NO₂) would also interact with
174 scrubbing solution in the second coil in a similar way as in the first coil. The nitrite solutions from the two coils
175 were then respectively mixed with sulfanilamide/N-(1-naphthyl) ethylene-diamine (SA/NED) reagents in Teflon
176 derivatization tubing and nitrite was converted via the two reactions (SR1 and SR2, see the SI for details) (Huang
177 et al., 2002). The aqueous sample was injected into the LWCC and the produced azo dye was quantified by its
178 absorption at 560 nm with a mini USB spectrometer. The difference between the absorbance signals of the two
179 coils was treated as the actual HONO signal. The HONO mixing ratio in ambient air was calculated using Eq. (1):

$$180 \quad [\text{HONO}]_{\text{pptv}} = \frac{C_1 F_1 R T}{F_g P} \times 10^{12} \quad (1)$$

181 where, C₁ is nitrite concentration (mol L⁻¹) in the scrubbing solution, F₁ is the liquid flow rate (mL min⁻¹) of the
182 scrubbing solution, F_g is the sampling air flow rate (L min⁻¹), R is the ideal gas constant (8.314 m³ Pa K⁻¹ mol⁻¹),
183 and T and P are the ambient temperature (294 K) and atmospheric pressure (101325 Pa), respectively, under which
184 the mass flow controller (MFC) that was used to control the sample flow rate was calibrated (Ren et al., 2010). The
185 instrument calibration was carried out once every four days by injecting standard sodium nitrite (NaNO₂) solution
186 into the instrument right after the sampling coil. According to the calibration curve, HONO mixing ratio in ambient

Deleted: The HONO instrument was calibrated every four days using sodium nitrite standard solutions.

189 air can be quantified. The detection limit of the HONO instrument was about 3 pptv with a time resolution of 2
190 min. The measurement accuracy was about $\pm 15\%$ at a 95% confidence level (Ren et al., 2010).

191 **2.2 Other measurements**

192 As the observation site was part of a national standard meteorology observatory facility, meteorology
193 parameters, including wind direction, wind speed, ambient temperature, pressure and RH were continuously
194 measured. Trace gases, CO (Thermo Scientific, Model 48i), O₃ (Thermo Scientific, Model 49i), SO₂ (Thermo
195 Scientific, Model 43i) and NO_x (Thermo Scientific, Model 17i) were also measured at the observation site. The
196 Thermo Scientific 17i is designed as an ammonia (NH₃) analyzer. It basically consists of a typical NO_x analyzer
197 and an external high temperature (700°C) NH₃ converter, which is disabled and bypassed in this work. Therefore,
198 it was used as a typical NO_x analyzer. It is well known that a NO-NO_x analyzer with a molybdenum-based converter
199 can convert portion of NO_z (=NO_y-NO_x) to NO, which can then be detected as NO₂ causing an interference in NO₂
200 measurement (Villena et al., 2012). However, an aircraft study conducted in the eastern US in the winter 2015
201 found that within 6 hours of transport time, NO_x account for more than 90% of NO_y in an urban outflow (Salmon
202 et al., 2018). A sensitivity analysis showed that by decreasing the NO₂ level of 10% (an upper limit assuming all
203 NO_z were converted into NO with an efficiency of 100%), the modeled HONO decreased only by 5.3%, indicating
204 that the possible small interference in NO₂ measurement did not impact significantly on the modeled HONO results.
205 The details about the operation and calibrations of these instruments were described in previous work (Zheng et al.,
206 2015b). PM_{2.5} was observed by an online PM_{2.5} measuring instrument (METONE, BAM-1020) with a time
207 resolution of 1 hour. Aerosol surface area density was calculated using data from an WPS (wide particle
208 spectrometer, MSP model 1000XP) with a time resolution of 5 min. HCHO was measured with the DNPH method
209 from 19 to 30 December 2015 and the sampling time was 2 hours during the campaign. Detailed operation
210 procedures about the DNPH method in this study can refer to our previous work (Ma et al., 2016). Photolysis

211 frequencies (J values), including J(O¹D), J(NO₂), J(HONO), J(H₂O₂), J(HCHO), and J(NO₃), were calculated based
212 on measurements by an ultra-fast charged coupled device (CCD) detector spectrometer (Meteorology Consult
213 Gmbh, Germany). The acquisition time for J values was 1 min. Other photolysis frequencies (such as carbonyls
214 with more than two carbons) used in the model were calculated by Eq. (2) (Jenkin et al., 1997):

$$215 \quad J_i = L_i \cos(\chi) M_i \exp(-N_i \sec(\chi)) \quad (2)$$

216 where χ is the solar zenith angle; L_i , M_i , and N_i are photolysis parameters and are taken from (Jenkin et al., 1997),
217 for clear sky conditions. The calculated photolysis frequencies were then scaled by the measured J(NO₂) for
218 cloudiness correction.

219 Volatile organic compounds (VOC) measurements were conducted using a commercial gas chromatograph
220 equipped with a flame ionization detector (GC-FID) (AMA, GC5000). Sixty VOC species including C₂-C₁₂
221 hydrocarbons were detected with a time resolution of 1 hr. Ten of the most reactive alkenes were used in the
222 ozonolysis reaction in the box model simulations. Although the oxygenated VOCs (OVOCs) other than
223 formaldehyde and some other carbonyls (by the DNPH method) were not measured in this study, they were
224 simulated in the box model that was constrained to measured VOCs. Our results indicated that OVOCs only
225 accounted for a small portion of the total VOCs in this industrial area and even contributed much less to the total
226 VOC OH reactivity. Therefore, the limited VOCs detected in this work would not significantly affect the following
227 model simulation results.

228 2.3 Box Model

229 To evaluate the effect of HONO on daytime atmospheric oxidation capacity, a chemical box model with the
230 Master Chemical Mechanism (MCMv3.2) (Jenkin et al., 2012) was applied to calculate the concentrations of OH,
231 HO₂ radicals and their production and loss rates using the FACSIMILE software package (UES Software Inc.).
232 Kinetic rate coefficients were taken from the MCM website (<http://mcm.leeds.ac.uk/MCM/>). In this study, the

233 model simulation was constrained with hourly averaged measurement results, including HONO, O₃, NO, NO₂, CO,
234 SO₂, HCHO, VOCs, as well as water vapor, temperature, pressure, and photolysis frequencies.

235 Monte Carlo sensitivity analyses were conducted to assess the model performance. In each Monte Carlo
236 simulation, the input variables of the model, including HONO, O₃, NO, NO₂, CO, SO₂, HCHO, VOCs, reaction
237 rate constants, photolysis frequencies [and the planetary boundary layer \(PBL\) height](#) were independently set to
238 vary within ±10% of the mean value of individual variable with a normal probability distribution.

239

240 **3 Results and Discussion**

241 **3.1 Data Overview**

242 Figure 2 shows the time series of NO, NO₂, O₃, PM_{2.5}, HONO, HCHO, J(HONO), and meteorological
243 parameters, including wind direction, wind speed, temperature, and RH. During the entire campaign period, the
244 wind speed ranged from 0.1 to 8.1 m s⁻¹ with an average of 1.7 m s⁻¹. The temperature varied between -4.1 and 16.1
245 °C with an average of 6.1 °C; RH varied [from 17 to 96](#) % with an average of 68 %.

246 During the entire measurement period, the HONO mixing ratios ranged from 0.03 to 7.04 ppbv with a mean
247 value of 1.32 ± 0.92 ppbv. Table 1 lists recent HONO observations conducted in China. Our result was comparable
248 to HONO observed in Xinken (Su et al., 2008) and Beijing (Spataro et al., 2013; Wang et al., 2017) but higher than
249 Xianghe, Beijing (Hendrick et al., 2014), Jinan (Wang et al., 2015a), Hong Kong (Xu et al., 2015) and Shanghai
250 (Wang et al., 2013). Clearly, the general trend of HONO was closely following that of NO₂, which is the dominant
251 precursor of HONO. More markedly, building up of HONO frequently proceeded the accumulations of PM_{2.5}, e.g.,
252 on the 7th and from the 21st - 22nd of December 2015, indicating that HONO may promote the formation of
253 secondary aerosol by contributing to OH production, which will be further analyzed in details in the following

254 sections. The campaign averaged diurnal variations of HONO, NO₂, HONO/NO₂ ratio and aerosol S/V are showed
255 in Fig. 3. HONO started to accumulate after sunset and reached its daily averaged maxima of ~2.0 ppbv at 08:00
256 local time (LT). Later the day, the HONO mixing ratio decreased rapidly due to its fast photolysis and increase of
257 the PBL height. Evidently, daytime HONO was sustained at a relatively high level. The daily averaged minimum
258 of ~0.6 ppbv was observed around 16:00 LT. The mixing ratio of NO₂ varied from 9.5 to 48.7 ppbv with an average
259 of 23.9 ± 7.5 ppbv and a daily averaged maximum of 27.7 ± 8.8 ppbv. NO, O₃ and PM_{2.5} mixing ratios were in the
260 range of 2.7 to 124.9 ppbv, 3 to 39 ppbv and 15 to 345 µg m⁻³, respectively. Meanwhile, the HONO-to-NO₂ ratios
261 ranged from 0.02 to 0.07, with an average of 0.05 ± 0.03. ▼

262 3.2 OH Simulation

263 Although atmosphere oxidation capacity is determined by the levels of all major oxidants in the atmosphere
264 (e.g., OH, O₃, and NO₃), OH radical is the primary oxidant in the atmosphere and series of reactions initiated by
265 OH radical can lead to the formation of other major secondary oxidants, such as O₃ and NO₃. Fully understanding
266 the budget of OH radical especially the sources of OH radical is of paramount importance for the purpose of
267 controlling the atmosphere oxidation capacity and hence to establish effective air pollution mitigation strategies.

268 *In-situ* measurement of OH radical is often limited by the availability of suitable measurement techniques,
269 which are often suffered from large amount of unresolved uncertainties (Tanner and Eisele, 1995) and the
270 observation often disagree with the modeling results to a large extent. Nevertheless, theoretically some critical
271 parameters to govern the OH radical budget in the atmosphere are difficult to measure directly, such as the
272 formation rates of OH. Accordingly, a box model is often utilized to simulate these highly reactive species to
273 investigate their photochemistry.

274 In order to assess the relative contributions of potential OH sources in this study, we have utilized a box model
275 based on the Master Chemical Mechanism (MCMv3.2) (Jenkin et al., 2012) to simulate the OH concentration and

Deleted: The observed similarity between the diurnal profile of HONO/NO₂ ratio and that of HONO suggested that HONO was likely originated from NO₂ heterogeneous reactions.

280 the OH formation rates from various sources. The model simulation was constrained by the measurement results,
281 including HONO, O₃, NO, NO₂, CO, SO₂, VOCs, as well as water vapor, temperature, pressure, and photolysis
282 frequencies. Since HCHO measurement was only available from 19 to 30 December, simulated HCHO was used
283 for the entire campaign period. We found that the ratio between simulated to measured HCHO was 1.4 with a
284 correlation coefficient of R = 0.77. Therefore, we applied a factor of 1.4 to the simulated HCHO in the model to
285 better represent the HCHO concentration in the atmosphere.

286 The simulated OH time series during the campaign period is shown in Fig. 4. Because the simulation is
287 constrained by the observations, only within periods when all data are available simulation were conducted.

288 Simulated OH concentration was in the range of 1.06×10^6 to 5.26×10^6 molecules cm⁻³, similar to the concentration
289 observed in London (Emmerson et al., 2007), but lower than that measured in New York City (3×10^6 to 3.3×10^7)
290 (Ren et al., 2003) and Guangzhou (1.5×10^7 to 2.6×10^7) (Lu et al., 2012).

291 It should be noted that the absolute values of the simulated OH may differ from the actual ambient
292 concentration. However, the general trend of OH evidently followed the solar radiation intensity, indicating its
293 photochemical production origin. Clearly, the diurnal variation of OH profile is more complicated than that of
294 photolysis rates because OH production can be affected not only by photochemical processes, but also by both
295 primary emissions (e.g., HONO and HCHO) and other non-photochemical related heterogeneous processes, such
296 as HONO production on various surfaces and ozonolysis of alkenes. These processes will be further discussed in
297 the following sections.

298 3.3 OH Formation Rates

$$299 \quad P_{OH}(HONO)_{net} = J(HONO)[HONO] - k_{OH+NO}[NO][OH] \quad (3)$$

$$300 \quad P_{OH}(O_3) = 2J(O^1D)[O_3]\phi_{OH} \quad (4)$$

$$301 \quad P_{OH}(HCHO) = 2J(HCHO)[HCHO] \quad (5)$$

302
$$P_{OH}(H_2O_2) = 2J(H_2O_2)[H_2O_2] \quad (6)$$

303
$$P_{OH}(O_3 + \textit{alkenes}) = \sum k_{\textit{alkene}(i)+O_3}[\textit{alkene}(i)][OH]Y_{OH,i} \quad (7)$$

304 Previous field studies have demonstrated that HONO photolysis can contribute substantially to the OH
 305 production during daytime (Elshorbany et al., 2009; Hendrick et al., 2014; Kleffmann et al., 2005; Su et al., 2008).
 306 In this study, we evaluated the OH formation rates from the photolysis of HONO (Eq. 3), ozone (Eq. 4),
 307 formaldehyde (Eq. 5) and hydrogen peroxide (H₂O₂) (Eq. 6), as well as ozonolysis of alkenes (Eq. 7). The second
 308 term in Eq. 3 is to account for the loss of OH due to the HONO formation from OH + NO, where the OH
 309 concentration was simulated using the box model, so that the net OH formation from the photolysis of HONO is
 310 considered. J values are the photolysis frequencies of the corresponding species and ϕ_{OH} is the fraction of O(¹D)
 311 reacts with H₂O instead of being quenched by nitrogen (N₂) or oxygen (O₂). The OH production by the photolysis
 312 of formaldehyde was calculated assuming that HO₂ formed from reaction R4 was immediately converted into OH
 313 by reaction R8 due to high NO levels in this polluted environment. In Eq. 7, Y_{OH,i} is the yield of OH from gas-
 314 phase reaction of O₃ and alkene(i) and $k_{\textit{alkene}(i)+O_3}$ is the reaction rate constant for the reaction of O₃ with alkene(i).
 315 The rate constants of the ozonolysis reactions and the corresponding OH yields used in this work are listed in Table
 316 2. Since H₂O₂ was not measured during this campaign, H₂O₂ was estimated from literature values, i.e., 0.5 to 5
 317 ppbv (Guo et al., 2014; Hua et al., 2008; Ren et al., 2009) and a constant of 3 ppbv H₂O₂ was used in this work.

318 The calculated campaign averaged OH production rates from the photolysis of HONO, O₃, HCHO and H₂O₂
 319 along with ozonolysis of alkenes were 7.13×10^6 , 2.46×10^6 , 1.60×10^6 , 2.39×10^5 and 3.94×10^6 molecules cm⁻³ s⁻¹,
 320 respectively, which were comparable with the literature values (Alicke et al., 2002; Chan et al., 2017; Su et al.,
 321 2008). As shown in Fig. 5, the contribution of HONO photolysis to OH production [during 7:00-16:00 local time](#)
 322 varied from 23.6 to 63.3% with a mean value of 44.8%. The ozonolysis of ten highly reactive alkenes (listed in
 323 Table 2) by ozone was the second largest contributor to OH radical and the contribution varied from 16.1 to 60.9%
 324 with a mean of 30.3%. The contribution of ozone photolysis was in the range of 1.3 to 24.7% with a mean of 14.9%.

325 The contribution of HCHO photolysis varied between 0.9 and 12.5% with a mean of 8.1%, and the contribution of
326 H₂O₂ photolysis was negligible with an average contribution of 1.9%. The contributions from different OH sources
327 in this study was similar to those found in two wintertime studies. In a study conducted in New York City in winter
328 2004, it was found that 48% of the net HO_x production was from the HONO photolysis, 36% from the ozonolysis
329 of alkenes, only 6% from the HCHO photolysis, and 1% from the O₃ photolysis (Ren et al., 2006). In another study
330 conducted in London in winter 2000, 62% of the OH production was found from the ozonolysis of alkenes, 35%
331 from the HONO photolysis, only 6% from the HCHO photolysis, and <1% from the O₃ photolysis (Heard et al.,
332 2004).

333 The striking features of the Fig. 5 is that HONO photolysis and ozonolysis of alkenes contributed more than
334 70% of the OH production rate on average. In the early morning, HONO photolysis was the dominant source of
335 OH and may boost the photochemistry right after sunrise. As O₃ accumulated, alkene ozonolysis and O₃ photolysis
336 became more and more important. The higher percentage of the HONO photolysis in this study is most likely
337 because of the higher concentrations of HONO observed in the study area and its sources will be further investigated
338 in the following sections.

339 **3.4 Industrial Plumes**

340 Industrial emissions are responsible for a large portion of the haze formation in China. With the
341 implementations of more and more strict mitigation strategies, primary emissions have been reduced substantially
342 in China. However, the observation site was located just ~5 km from the Nanjing industry park, one of the largest
343 industrial zones in the YRD region, which is populated with various heavy industry facilities, including steel mills,
344 power generation stations, and petrochemical refineries. Despite the great effort to reduce primary industrial
345 emissions from these facilities, industrial plumes have often been detected at the site, carrying fair amounts of NH₃,
346 NO_x, SO₂, and VOCs (Ma et al., 2016; Zheng et al., 2015a). To investigate the effects of industrial emissions on

347 local and regional air quality and particularly the role of HONO on the transformation of primary emissions into
348 secondary air pollutants, we have paid special attention into the air masses originated from the industrial zone.
349 Figure 6 depicts the contribution fractions of OH production rates from HONO photolysis, alkene ozonolysis, O₃
350 photolysis, HCHO photolysis, and H₂O₂ photolysis during two industrial plume events. The wind rose plots in Fig.
351 6 indicate that the origins of these air masses were all from the nearby industry zone. Unlike that depicted in Fig.
352 5, during the two industry pollution events HONO photolysis along with ozonolysis of alkenes dominated the OH
353 production throughout the day. This was most likely due to the high concentrations of NO_x and VOC within the
354 industrial plumes. More interestingly, the average PM_{2.5} concentrations during the two events were 139 and 239 μg
355 m⁻³, respectively. Evidently, HONO photolysis and ozonolysis may even play a more important role in OH
356 production during severe haze events. Although ambient OH concentrations during these events may not be high
357 (see Fig. 4a), the high levels of HONO can boost active photochemical oxidation and thus promote the formation
358 of ~~other secondary air pollutants.~~

Deleted: PM_{2.5}, which in turn provides additional reaction surface for more HONO production. To further test this hypothesis, we have investigated the HONO budgets in much details in the next section.

359 3.5 HONO Sources

360 3.5.1 Primary HONO Emissions

361 Previous studies have demonstrated that HONO can be emitted directly from vehicle exhaust (Kirchstetter et
362 al., 1996; Kurtenbach et al., 2001). ~~However~~, the NO/NO_x ratio measured in this work was relatively low, with an
363 average of 0.25±0.06, much less than that of freshly emitted exhausts (> 0.9) obtained from tunnel experiments
364 (Kurtenbach et al., 2001), indicating that the air masses sampled in this work had been considerably aged and mixed
365 with other air masses, and hence primary HONO ~~from direct emissions~~ (if there was any) had been diluted
366 substantially (less than a few per cents) before reaching the observation site. In addition, our sampling site is located
367 nearby the industrial zone, and the high concentration of NO_x was mainly originated from the industrial activities,
368 so the influence of traffic source on HONO was expected to be ~~small. To further evaluate the potential impact of~~

Deleted: negligible

374 primary emissions on HONO concentration, we have incorporated the contribution of primary HONO emissions
375 into the MCM box model. The HONO emission ratios, i.e., HONO/NO_x, was taken as 0.3% (Kirchstetter et al.,
376 1996), representing a gasoline-fueled vehicle fleet, which was very typically encountered in the study area. On
377 average, the primary emissions from vehicle exhaust can only account for 11% of the total HONO concentration,
378 indicating secondary mechanisms still dominated HONO level in the study area, which will be further analyzed in
379 the following sections.

380 3.5.2 HONO Conversion Rate

381 In addition to primary emission, heterogeneous reactions of NO₂ on surfaces are believed to be the major
382 formation pathways of nocturnal HONO. In order to discuss the influence of secondary mechanisms on HONO,

383 the observed HONO was corrected by removing the portion of primary emission (HONO_{emis}) and was denoted as

384 HONO_{corr} (= HONO - HONO_{emis}).

385 The HONO conversion rate k(het) (hr⁻¹) is an important parameter to compare HONO formation under various
386 NO₂ levels (Xu et al., 2015). In this work, we calculate the HONO conversion rate using the Eq. (8) (Alicke et al.,
387 2003):

$$388 \quad k(\text{het}) = \frac{[\text{HONO}_{\text{corr}}]_{t_2} - [\text{HONO}_{\text{corr}}]_{t_1}}{(t_2 - t_1)[\text{NO}_2]} \quad (8)$$

389 where [HONO_{corr}]_{t₁} and [HONO_{corr}]_{t₂} are the corrected HONO concentrations at two different times, t₁ and t₂,
390 respectively, [NO₂] is the average NO₂ concentration between time t₁ and t₂. The time periods used to calculate
391 HONO/NO₂ conversion ratio were selected when both HONO and NO₂ increased monotonically with a correlation
392 coefficient higher than 0.8. Note Eq. (8) is a simplified demonstration to calculate the reaction rate coefficient of

393 the heterogeneous conversion from NO₂ to HONO at night, which can be dependent on different pollution levels.

394 In this study, the averaged k(het) was determined to be ~0.8% hr⁻¹, which was comparable to the results in the urban
395 sites of Xi'an (0.91% hr⁻¹) (Huang et al., 2017) and Shanghai (0.7% hr⁻¹), China (Wang et al., 2013), but much less

Deleted: HONO

Deleted: HONO

398 than some other observations, such as Back Garden, Guangdong, China (2.4% hr⁻¹) (Li et al., 2012), Xinken,
399 Guangdong, China (1.6% hr⁻¹) (Li et al., 2012) and Rossfeld, Rhine Valley, France (2.2% hr⁻¹) (Acker and Möller,
400 2007). Nevertheless, the high level of NO_x observed in this work may still lead to high level of HONO through
401 various mechanisms.

402 3.5.3 Heterogeneous Conversion of NO₂

403 Previous studies have suggested that heterogeneous conversion of NO₂ on wet surfaces could be an important
404 nocturnal HONO source (Finlayson-Pitts et al., 2003; Wang et al., 2017). However, it appears that the proposed
405 reaction mechanism (2NO₂ + H₂O) was limited by the uptake of NO₂ on the wet surfaces (on the order of 10⁻⁶) and
406 thus was too slow to account for the observed NO₂ to HONO conversion ratio (Kleffmann et al., 1998). Instead,
407 the reaction between NO₂ and adsorbed semi-volatile organic compounds on soot or aerosol surfaces has been
408 suggested to be one to two orders of magnitudes faster than the aforementioned reaction (George et al., 2005;
409 Gutzwiller et al., 2002) even though the actual reaction mechanism is still under active research. It also should be
410 noted that during nighttime as ambient temperature decreased, the PBL height also decreased, causing the ground
411 surface to air volume ratio to increase, which may also contribute to higher NO₂ to HONO conversion efficiency
412 (Stutz et al., 2004). However, as shown in Fig. 7, HONO_{corr}/NO₂ correlated with S/V to some extent and the
413 correlation increased with the product of RH and S/V. Therefore, even though the contribution of HONO formation
414 on the ground surface was present, the aerosol surface was certainly involved in the HONO formation process. The
415 impact of RH on the heterogeneous formation of HONO was further investigated. Figure 8 shows the relationship
416 between HONO_{corr}/NO₂ ratio and RH at night. The linearity of the bin points clearly displays the linear correlations
417 between HONO conversion ratio and RH. Following the method introduced by Stutz et al. (2004), we plotted the
418 top-5 values of HONO_{corr}/NO₂ ratio (representing steady state conditions) in each 10% RH interval. The conversion
419 efficiency of NO₂ to HONO correlates very well with RH (R=0.98), strongly indicating the dependence of HONO

Deleted: Figure 7 shows the correlation analyses for several individual days between HONO/NO₂ and RH, S/V, and the product of RH-S/V. For instance, on 25 December 2015, HONO correlated with RH (R² = 0.63) and S/V (R² = 0.70) to some extent. However, the correlations between HONO/NO₂ and the products of RH-S/V (R² = 0.77) was substantially improved, which was consistent with the participation of water in heterogeneous HONO formation during nighttime, particularly on the aerosol surfaces. These results were generally in line with the results of Stutz et al. (2004).

431 formation on RH. Similar phenomenon was also observed at an urban site (Qin et al., 2009) and a rural site (Li et
 432 al., 2012) in Guangzhou, China.

433 3.5.4 Daytime HONO Budget

434 High concentrations of daytime HONO were frequently observed during the campaign period especially
 435 within industrial plumes. If we assume HONO was in photostationary state involving only gas-phase homogeneous
 436 HONO production and photolysis loss, the calculated daytime HONO concentration would be 8.1×10^9 molecules
 437 cm^{-3} , only 24.5% of the observed mean HONO concentration during daytime. Since the gas phase reaction between
 438 OH and NO (i.e., $P_{\text{OH}+\text{NO}}$) [and primary emission \(\$P_{\text{emission}}\$ \)](#) were unable to explain the observed high HONO
 439 concentrations, daytime HONO budget was further examined in details. Here we designate the unexplained HONO
 440 source as P_{unknown} . The [temporal](#) variation of measured HONO concentration can be expressed by the following
 441 equation (Wang et al., 2017):

$$442 \quad \frac{d[\text{HONO}]}{dt} = (P_{\text{OH}+\text{NO}} + P_{\text{emissions}} + P_{\text{unknown}}) - (L_{\text{OH}+\text{HONO}} + L_{\text{photolysis}} + L_{\text{deposition}})$$

443 (9)

444 Thus, P_{unknown} can be calculated as:

$$445 \quad P_{\text{unknown}} = \frac{d[\text{HONO}]}{dt} + L_{\text{OH}+\text{HONO}} + L_{\text{photolysis}} + L_{\text{deposition}} - P_{\text{OH}+\text{NO}} - P_{\text{emission}}$$

$$446 \quad = \frac{d[\text{HONO}]}{dt} + k_{\text{OH}+\text{HONO}}[\text{OH}][\text{HONO}] + J_{\text{HONO}}[\text{HONO}] + \frac{v_{\text{HONO}}}{H}[\text{HONO}]$$

$$447 \quad - k_{\text{OH}+\text{NO}}[\text{OH}][\text{NO}] - \frac{0.003\Delta\text{NO}x}{\Delta t} \quad (10)$$

448 where $\frac{d[\text{HONO}]}{dt}$ represents the variation of observed HONO concentrations; $L_{\text{photolysis}}$ represents the loss rate of
 449 HONO by photolysis and J_{HONO} is the measured photolysis frequency of HONO; $P_{\text{NO}+\text{OH}}$ and $L_{\text{OH}+\text{HONO}}$ are the gas-
 450 phase formation and loss rates of HONO, respectively; $k_{\text{OH}+\text{NO}}$ and $k_{\text{OH}+\text{HONO}}$ are the corresponding reaction rate
 451 constants; $L_{\text{deposition}}$ is the dry deposition rate of HONO; v_{HONO} represents deposition velocity of HONO and H is
 452 the mixing height; [the last term represents direct emissions of HONO](#). For v_{HONO} , a value of 0.48 cm s^{-1} was

453 adopted (Lee et al., 2016) and the observed mixing height varied from 73 m to 600 m diurnally. A sensitivity
454 analysis with and without the HONO deposition shows that the modeled HONO concentration with HONO
455 deposition loss is 3.5% lower than that without HONO deposition during daytime, indicating that the dry deposition
456 of HONO plays a minor role in HONO losses. The impact of HONO direct emissions was relatively small at
457 daytime. Daytime OH concentration was not measured in this work but was simulated by the MCM box model.

458 Figure 9 shows the average diurnal variation of each individual term in Eq. (10). Compared with $L_{\text{photolysis}}$, the
459 gas-phase reaction between OH and HONO and HONO dry deposition contributed very little to the HONO sink
460 during daytime. However, $P_{\text{OH+NO}}$ and P_{unknown} both contributed significantly to the HONO production and displayed
461 a completely distinct diurnal pattern. Homogeneous reaction between OH and NO reached a maximum of 1.04
462 ppbv hr⁻¹ in the early morning (09:00 LT) due to high concentrations of NO in the morning. The unknown source
463 reached a maximum of 1.22 ppbv hr⁻¹ around noontime with an average of 0.73 ppbv hr⁻¹, which was about twice
464 as much as averaged $P_{\text{OH+NO}}$. The diurnal profile of P_{unknown} showed a strong photo-enhanced feature, which is
465 consistent with that observed by Michoud et al. (2014) in wintertime Europe.

466 3.5.5 Photo-Enhanced Conversion of NO₂

467 The nature of the unknown source was explored by correlation analyses between P_{unknown} and other HONO
468 production related parameters (see Table 3). P_{unknown} does not correlate well with RH, NO₂, S/V, and J_{NO_2} with the
469 correlation coefficients (R) of 0.27, 0.31, 0.33, and 0.31 respectively. The correlation increased only slightly when
470 heterogeneous conversion of NO₂ (NO₂-RH, R = 0.40) was taken into consideration. It appeared that the unknown
471 HONO sources cannot be well explained by the heterogeneous reactions on wet surfaces alone. Previous studies
472 have suggested that light intensity could be an important parameter influencing the heterogeneous conversion of
473 NO₂ to HONO (Han et al., 2017b; Lee et al., 2016). The photo-enhanced HONO source during the daytime has
474 also been identified in different environments ranging from remote (Villena et al., 2011; Zhou et al., 2002) to urban

475 conditions (Lee et al., 2016). When photo-enhancement was also considered ($J_{\text{NO}_2 \cdot \text{NO}_2 \cdot \text{RH}}$, $R = 0.70$), a
476 significantly better correlation was achieved (Table 3). This suggests that the photosensitized reaction of NO_2 on
477 wet surfaces may be an important source of HONO during daytime. Thus, the improvement in the correlation
478 between HONO and other parameters indicates that photochemistry might indeed play an important role in daytime
479 HONO formation (George et al., 2005; Stemmler et al., 2006). Since the correlation coefficient between P_{unknown} and
480 $J_{\text{NO}_2 \cdot \text{NO}_2 \cdot \text{RH}}$ is comparable with the value between P_{unknown} and $J_{\text{NO}_2 \cdot \text{NO}_2 \cdot \text{S/V} \cdot \text{RH}}$ ($R = 0.70$), either ground or
481 aerosol surfaces can be the dominant reaction site for photosensitized conversion of NO_2 .

482 Since aerosol chemical composition was not measured in this work, we cannot demonstrate any possible direct
483 connection between aerosol composition and the photo-enhanced HONO formation on aerosol surfaces.
484 Nevertheless, the actual mechanism underlying the photo-enhanced HONO formation on aerosol surface needs
485 further investigation. It has been found that photo-sensitized NO_2 conversion rate coefficient on different surfaces
486 can vary substantially (Han et al., 2017a; Stemmler et al., 2006). Furthermore, studies have shown that this type of
487 surface reaction is not catalytic in nature and the surface reaction rate may vary with the availability and aging state
488 of the surface reaction sites (Stemmler et al., 2006). Therefore, aerosol chemical composition alone may not be
489 sufficient to reveal the actual HONO formation processes.

490 3.5.6 Model Simulation of HONO

491 The relative contributions of potential HONO sources were assessed by a box model based on the Master
492 Chemical Mechanism (MCMv3.2) (Jenkin et al., 2012). In addition to the homogeneous reaction of NO with OH ,
493 four sources of HONO were included, i.e., heterogeneous HONO formation from NO_2 reaction on aerosol surface
494 and ground surface and light-induced conversion of NO_2 on aerosols and ground surface. Dry deposition of HONO
495 was also considered and a deposition velocity of 0.48 cm s^{-1} was used here (Lee et al., 2016).

496 Most laboratory studies suggest that the heterogeneous reaction on surface leading to HONO is proportional

497 to the first order of NO₂ (Finlayson-Pitts and Pitts, 1999), therefore the HONO formation can be represented by the
 498 following reactions (Li et al., 2010):



501 where k_a and k_g are the first-order rate constants for aerosol and ground surface reactions, respectively. For the
 502 heterogeneous reaction on aerosols, the first order rate constant was estimated as:

$$503 \quad k_a = \frac{\gamma_{\text{NO}_2, \text{aerosol}} \bar{v} (S/V)}{4} \quad (13)$$

504 where \bar{v} is the root mean square (RMS) velocity of NO₂, S/V is the aerosol surface area-to-volume ratio and
 505 $\gamma_{\text{NO}_2, \text{aerosol}}$ is the reactive uptake coefficient on the aerosol surface, with a value of 1×10^{-6} under dark conditions
 506 (Aumont et al., 2003; Li et al., 2010). Under sunlight, however, significant enhancement of NO₂ conversion to
 507 HONO has been found for various types of aerosol surfaces, such as humic acid and similar organic materials
 508 (Stemmler et al., 2007), soot (Monge et al., 2010), and mineral dusts (Ndour et al., 2008). To account for the
 509 photoenhancement, a higher value of uptake coefficient (2×10^{-5}) was used for solar radiation less than 400 W m^{-2}
 510 and an uptake coefficient scaled by (light intensity)/400 for solar radiation larger than 400 W m^{-2} as suggested by
 511 Li et al. (2010). Accordingly, in this work the photoenhanced uptake coefficient was taken as 2×10^{-5} around the
 512 morning hours (~9 AM) and was scaled by the measured photolysis rate of NO₂, i.e., $(J_{\text{NO}_2}) / 2 \times 10^{-3}$ for J_{NO_2} higher
 513 than 2×10^{-3} (the value of J_{NO_2} at ~9 AM).

$$514 \quad k_g = \frac{V_{d, \text{NO}_2}}{2H} \quad (14)$$

$$515 \quad V_{d, \text{NO}_2} = \frac{\gamma_{\text{NO}_2, \text{ground}} \bar{v}}{4.2} \quad (15)$$

516 Equation (14) was used to denote the heterogeneous reactions on the ground surfaces, where V_{d, NO_2} represents
 517 deposition velocity of NO₂; H is the PBL height; and $\gamma_{\text{NO}_2, \text{ground}}$ is the reactive uptake coefficient on the ground.
 518 Here we assume an NO₂ reactive uptake coefficient of 1×10^{-5} (Trick, 2004) in the dark on ground surfaces with a
 519 yield of 50% and increase it to 2×10^{-5} in the daytime, given that the photosensitized reactivity of NO₂ on the ground

520 surface is the same as on the aerosol surface. The observed boundary layer height varied from 73 m to 600 m
521 diurnally. The same scale factor ($(JNO_2)/2 \times 10^{-3}$) was also applied to the daytime ground surface reactions.

522 Figure 10a shows the averaged diurnal profiles of the measured HONO concentration and the simulated
523 HONO concentrations from different sources. In general, the box model can capture the observed HONO trend
524 with very similar magnitude of concentration, with a modeled-to-observed HONO ratio of 1.26 during the day and
525 1.66 at night. In early morning, ground surface appeared to play an important role in HONO heterogeneous
526 production while the PBL was still relatively shallow. However, after ~9:00, despite of the swift developing of PBL,
527 fine particle loading started increasing substantially (as shown in Fig. 3), indicating strong secondary formation of
528 aerosols. Meanwhile, HONO production on aerosol surfaces also increased moderately. We found that higher
529 daytime values were mostly due to the light-induced conversion of NO_2 on aerosol surfaces in addition to the
530 homogeneous reaction of NO with OH. While at night, heterogeneous HONO production on ground surface
531 dominated nocturnal HONO sources and the nighttime aerosol surfaces only contributed slightly (2.2% and 7.9%,
532 respectively) to the total nighttime HONO. The box model tended to under-predict HONO during daytime, which
533 also led to a ~1-hr delay in the peaking time of the simulated HONO. The most likely reason for these disagreements
534 is due to the fact that heterogeneous conversion of NO_2 on various surfaces is too complicated to be fully
535 represented by a single scaling parameter in a linear form. Nevertheless, the general agreement between observation
536 and simulation in this work demonstrated that photo-induced NO_2 conversion on aerosol surfaces was the most
537 important HONO source in the study area during daytime.

538 A Monte Carlo sensitivity analysis was also conducted to assess the model simulation uncertainty of HONO
539 concentration. For each of the 24 hours, 100 independent runs were performed. The Monte Carlo sensitivity
540 analysis show that the model uncertainty of HONO ranged from $\pm 13\%$ to $\pm 38\%$. The sensitivity analysis reinforced
541 the conclusions that the proposed heterogeneous sources can generally capture the observed HONO trend.

542 To investigate the interaction between HONO chemistry and secondary aerosol formations within industrial

543 plumes, we have simulated HONO within the two industrial plume events (see Fig. 6). The results are shown in
544 Fig. 10b. Clearly, HONO was much higher within the industrial plumes comparing to the campaign average (Fig.
545 10a). In addition, we have performed a model sensitivity study with respect to aerosol surface density by varying
546 S/V from 50% to 200% of the average value. The results showed that the contribution from heterogeneous
547 photosensitized conversion of NO₂ on aerosol surfaces would correspondingly vary from 18% to 40% of the total
548 HONO budget, demonstrating that aerosol surface chemistry played an important role during HONO formation in
549 the study area. Indeed, aerosol surfaces were the most important HONO source during daytime (7:00 -16:00 LT),
550 especially in the afternoon. Within the industrial plumes, aerosol surfaces contributed around 35% of the observed
551 daytime HONO and only about 11% of total HONO was from the ground surfaces. The fact that ground surfaces
552 were less important during daytime than nighttime was most likely due to the much higher daytime PBL, causing
553 substantial dilution of HONO formed on the ground surfaces. Meanwhile, secondary particulate matters were
554 rapidly produced within the PBL, providing additional heterogeneous reaction sites for HONO formation as a
555 strong OH source to further promote atmospheric oxidative capacity. It should be noted that the reactive uptake of
556 NO₂ on various surfaces can be highly variable with the type of surfaces. The value used here ($\sim 2 \times 10^{-5}$) is toward
557 the lower end of values reported in the literatures, which is likely the reason that the simulated HONO is generally
558 less than the observations within industrial plumes. The heterogeneous NO₂ uptake kinetics and HONO yields of
559 real atmospheric substrates are still under active study and may be different compared to the artificial surfaces
560 studied in the laboratory setting. Nevertheless, enhanced photosensitized conversion of NO₂ on aerosol surfaces is
561 demonstrated here as a major HONO source in the plumes influenced by industrial emissions.

562

563 **4 Conclusions**

564 Nitrous acid was measured with a custom-built wet-chemistry based HONO analyzer, together with other
565 atmospheric OH precursors (O_3 and HCHO) at a suburb site of Nanjing in December 2015. The mixing ratios of
566 HONO varied from 0.03 ppbv to 7.04 ppbv with an average of 1.32 ± 0.92 ppbv. Daytime HONO was sustained at
567 a relatively high concentration, with a minimum diurnal hourly average of ~ 0.6 ppbv observed around 16:00 LT. A
568 MCM-box model was used to investigate the HONO chemistry and its impact on atmospheric oxidation capacity
569 in the study area. The results show that the average OH production rates from the photolysis of HONO, ozonolysis
570 of alkenes, photolysis of O_3 , HCHO, and H_2O_2 were 7.13×10^6 , 3.94×10^6 , 2.46×10^6 , 1.60×10^6 and 2.39×10^5
571 molecules $cm^{-3} s^{-1}$, respectively. The box model results show that the average total OH production rate was
572 1.54×10^7 molecules $cm^{-3} s^{-1}$ during daytime, on average about 45% from the photolysis of HONO, 30% from
573 ozonolysis of alkenes, 15% from the photolysis of O_3 , 8% from the photolysis of HCHO and 2% from the photolysis
574 of H_2O_2 .

575 Elevated daytime HONO evidently played an important role in sustaining the atmospheric oxidative capability
576 in the study area, which cannot be explained by the typical OH+NO homogeneous formation mechanism. The
577 observed similarity between the diurnal profiles of HONO/ NO_2 ratio and HONO strongly suggests that HONO was
578 most likely originated from NO_2 heterogeneous reactions. In this study, the averaged NO_2 to HONO conversion
579 rate was determined to be $\sim 0.8\% hr^{-1}$ at night. Good correlation between nocturnal HONO/ NO_2 and the products of
580 S/V·RH supports the heterogeneous NO_2/H_2O reaction mechanism.

581 To fully assess the HONO chemistry in the study area, an MCM box model was developed to examine HONO
582 budget. In general, the box model can capture the observed HONO trend with a modeled-to-observed HONO ratio
583 of 1.26 during the day and 1.66 at night. The model suggests that higher daytime levels of HONO were mainly
584 produced by the light-induced conversion of NO_2 on aerosol surfaces (28.2%) and ground surfaces (17.8%) (except

585 early morning). While the heterogeneous HONO production on ground surface dominated nocturnal HONO
586 sources, heterogeneous reactions on various surfaces only contributed a small portion of total HONO at daytime
587 (2.2% on aerosol surface and 7.9% on ground surface). The box model tends to over-predict HONO at night. The
588 most possible reason for these discrepancies is due to the fact that heterogeneous conversion of NO₂ on various
589 surfaces was too complicated to be fully represented by a single scaling parameter in a linear form. Nevertheless,
590 the general agreement between observation and simulation in this work reiterated that photo-induced NO₂
591 conversion on ground and aerosol surfaces was the most important HONO source in the study area. In the industrial
592 plume case study, it was demonstrated that heterogeneous photosensitized conversion of NO₂ on aerosol surfaces
593 was particularly intensified, when rapid growth of secondary particulate matter was simultaneously observed. Our
594 results indicate that the heterogeneous photosensitized conversion of NO₂ on aerosol surfaces becomes the largest
595 HONO source throughout the daytime, which in turn can enhance OH production, increase the oxidative capacity
596 of atmosphere, and further strengthen the formation of SOA during the daytime in this environment.

597

598 ***Author contributions***

599 JZ, YM, and XR designed the experiments, and XS, HJ, YG, WW, YZ, WZ, and YD carried out the field
600 measurements and data analysis. XS and XR performed the MCM box model simulation. JZ, XS, and YM prepared
601 the manuscript with comments from all coauthors.

602 ***Acknowledgements***

603 This work was supported by the National Natural Science Foundation of China (Grant numbers 41730106,
604 41575122, and 41675126) and the National Key Research and Development Project (Grant number
605 2017YFC0209501). The data used here are listed in the tables, figures, and the supporting materials.

606

607 **References**

608 Acker, K., Möller, D., Wieprecht, W., Meixner, F. X., Bohn, B., Gilge, S., Plass-Dülmer, C., and Berresheim, H.:
609 Strong daytime production of OH from HNO₂ at a rural mountain site, *Geophys. Res. Letts.*, 33, L02809,
610 10.1029/2005GL024643, 2006.

611 Acker, K., and Möller, D.: Atmospheric variation of nitrous acid at different sites in Europe, *Environ. Chem.*, 4,
612 242-255, <https://doi.org/10.1071/EN07023>, 2007.

613 Aliche, B., Platt, U., and Stutz, J.: Impact of nitrous acid photolysis on the total hydroxyl radical budget during the
614 Limitation of Oxidant Production/Pianura Padana Produzione di Ozono study in Milan, *J. Geophys. Res. Atmos.*,
615 107, 8196, 10.1029/2000JD000075, 2002.

616 Aliche, B., Geyer, A., Hofzumahaus, A., Holland, F., Konrad, S., Patz, H. W., Schafer, J., Stutz, J., Volz-Thomas,
617 A., and Platt, U.: OH formation by HONO photolysis during the BERLIOZ experiment, *J. Geophys. Res. Atmos.*,
618 108, 17, 8247
619 10.1029/2001jd000579, 2003.

620 Ammann, M., Kalberer, M., Jost, D. T., Tobler, L., Rossler, E., Pignatelli, D., Gaggeler, H. W., and Baltensperger, U.:
621 Heterogeneous production of nitrous acid on soot in polluted air masses, *Nature*, 395, 157-160, 10.1038/25965,
622 1998.

623 Atkinson, R., and Arey, J.: Atmospheric degradation of volatile organic compounds, *Chem. Rev.*, 103, 4605-4638,
624 10.1021/cr0206420, 2003.

625 Aumont, B., Chervier, F., and Laval, S.: Contribution of HONO sources to the NO_x/HO_x/O₃ chemistry in the
626 polluted boundary layer, *Atmos. Environ.*, 37, 487-498, [https://doi.org/10.1016/S1352-2310\(02\)00920-2](https://doi.org/10.1016/S1352-2310(02)00920-2), 2003.

627 Bernard, F., Cazaunau, M., Gosselin, B., Zhou, B., Zheng, J., Liang, P., Zhang, Y., Ye, X., Daele, V., Mu, Y., Zhang,
628 R., Chen, J., and Mellouki, A.: Measurements of nitrous acid (HONO) in urban area of Shanghai, China, *Environ.*
629 *Sci. Pollut. Res. Int.*, 23, 5818-5829, 10.1007/s11356-015-5797-4, 2016.

630 Chan, K. L., Wang, S., Liu, C., Zhou, B., Wenig, M. O., and Saiz-Lopez, A.: On the summertime air quality and
631 related photochemical processes in the megacity Shanghai, China, *Sci. Total Environ.*, 580, 974-983,
632 <https://doi.org/10.1016/j.scitotenv.2016.12.052>, 2017.

633 Ding, A. J., Fu, C. B., Yang, X. Q., Sun, J. N., Zheng, L. F., Xie, Y. N., Herrmann, E., Nie, W., Petäjä, T., Kerminen,
634 V. M., and Kulmala, M.: Ozone and fine particle in the western Yangtze River Delta: an overview of 1 yr data at
635 the SORPES station, *Atmos. Chem. Phys.*, 13, 5813-5830, 10.5194/acp-13-5813-2013, 2013.

636 Elshorbany, Y. F., Kurtenbach, R., Wiesen, P., Lissi, E., Rubio, M., Villena, G., Gramsch, E., Rickard, A. R., Pilling,
637 M. J., and Kleffmann, J.: Oxidation capacity of the city air of Santiago, Chile, *Atmos. Chem. Phys.*, 9, 2257-2273,
638 10.5194/acp-9-2257-2009, 2009.

639 Elshorbany, Y. F., Kleffmann, J., Kurtenbach, R., Lissi, E., Rubio, M., Villena, G., Gramsch, E., Rickard, A. R.,
640 Pilling, M. J., and Wiesen, P.: Seasonal dependence of the oxidation capacity of the city of Santiago de Chile,
641 *Atmos. Environ.*, 44, 5383-5394, 10.1016/j.atmosenv.2009.08.036, 2010.

642 Elshorbany, Y. F., Steil, B., Brühl, C., and Lelieveld, J.: Impact of HONO on global atmospheric chemistry
643 calculated with an empirical parameterization in the EMAC model, *Atmos. Chem. Phys.*, 12, 9977-10000,
644 10.5194/acp-12-9977-2012, 2012.

645 Emmerson, K. M., Carslaw, N., Carslaw, D. C., Lee, J. D., McFiggans, G., Bloss, W. J., Gravestock, T., Heard, D.
646 E., Hopkins, J., Ingham, T., Pilling, M. J., Smith, S. C., Jacob, M., and Monks, P. S.: Free radical modelling studies
647 during the UK TORCH Campaign in Summer 2003, *Atmos. Chem. Phys.*, 7, 167–181, doi:10.5194/acp-7-167-
648 2007, 2007.

649 Finlayson-Pitts, B. J., and Pitts, J. N.: *Chemistry of the upper and lower atmosphere : theory, experiments and*
650 *applications*, Academic Press, San Diego, Calif., xxii, 969 pp., 1999.

651 Finlayson-Pitts, B. J., Wingen, L. M., Sumner, A. L., Syomin, D., and Ramazan, K. A.: The heterogeneous
652 hydrolysis of NO₂ in laboratory systems and in outdoor and indoor atmospheres: An integrated mechanism, *PCCP*,
653 5, 223-242, 10.1039/b208564j, 2003.

654 Gall, E. T., Griffin, R. J., Steiner, A. L., Dibb, J., Scheuer, E., Gong, L., Rutter, A. P., Cevik, B. K., Kim, S., Lefer,
655 B., and Flynn, J.: Evaluation of nitrous acid sources and sinks in urban outflow, *Atmos. Environ.*, 127, 272-282,
656 10.1016/j.atmosenv.2015.12.044, 2016.

657 George, C., Strekowski, R. S., Kleffmann, J., Stemmler, K., and Ammann, M.: Photoenhanced uptake of gaseous
658 NO₂ on solid organic compounds: a photochemical source of HONO?, *Faraday Discuss.*, 130, 195-210,
659 10.1039/B417888M, 2005.

660 Gerecke, A., Thielmann, A., Gutzwiller, L., and Rossi, M. J.: The chemical kinetics of HONO formation resulting
661 from heterogeneous interaction of NO₂ with flame soot, *Geophys. Res. Letts.*, 25, 2453-2456, 10.1029/98GL01796,
662 1998.

663 Gherman, T., Venables, D. S., Vaughan, S., Orphal, J., and Ruth, A. A.: Incoherent Broadband Cavity-Enhanced
664 Absorption Spectroscopy in the near-Ultraviolet: Application to HONO and NO₂, *Environ. Sci. Technol.*, 42, 890-
665 895, 10.1021/es0716913, 2008.

666 Guo, J., Tilgner, A., Yeung, C., Wang, Z., Louie, P. K. K., Luk, C. W. Y., Xu, Z., Yuan, C., Gao, Y., Poon, S.,
667 Herrmann, H., Lee, S., Lam, K. S., and Wang, T.: Atmospheric Peroxides in a Polluted Subtropical Environment:
668 Seasonal Variation, Sources and Sinks, and Importance of Heterogeneous Processes, *Environ. Sci. Technol.*, 48,
669 1443-1450, 10.1021/es403229x, 2014.

670 Gutzwiller, L., Arens, F., Baltensperger, U., Gäggeler, H. W., and Ammann, M.: Significance of Semivolatile Diesel
671 Exhaust Organics for Secondary HONO Formation, *Environ. Sci. Technol.*, 36, 677-682, 10.1021/es015673b, 2002.

672 Han, C., Liu, Y., and He, H.: Heterogeneous reaction of NO₂ with soot at different relative humidity., *Environ. Sci.*
673 *Pollut. Res.*, 24, 21248–21255, 10.1007/s11356-017-9766-y, 2017a.

674 Han, C., Yang, W., Yang, H., and Xue, X.: Enhanced photochemical conversion of NO₂ to HONO on humic acids
675 in the presence of benzophenone, *Environ. Pollut.*, 231, 979-986, <https://doi.org/10.1016/j.envpol.2017.08.107>,
676 2017b.

677 Heard, D. E., Carpenter, L. J., Creasey, D. J., Hopkins, J. R., Lee, J. D., Lewis, A. C., Pilling, M. J., Seakins, P. W.,
678 Carslaw, N., and Emmerson, K. M.: High levels of the hydroxyl radical in the winter urban troposphere, *Geophys.*
679 *Res. Letts.*, 31, 10.1029/2004gl020544, 2004.

680 Heland, J., Kleffmann, J., Kurtenbach, R., and Wiesen, P.: A New Instrument To Measure Gaseous Nitrous Acid
681 (HONO) in the Atmosphere, *Environ. Sci. Technol.*, 35, 3207-3212, 10.1021/es000303t, 2001.

682 Hendrick, F., Müller, J. F., Clémer, K., Wang, P., De Mazière, M., Fayt, C., Gielen, C., Hermans, C., Ma, J. Z.,
683 Pinardi, G., Stavrou, T., Vlemmix, T., and Van Roozendaal, M.: Four years of ground-based MAX-DOAS
684 observations of HONO and NO₂ in the Beijing area, *Atmos. Chem. Phys.*, 14, 765-781, 10.5194/acp-14-765-2014,
685 2014.

686 Hofzumahaus, A., Rohrer, F., Lu, K., Bohn, B., Brauers, T., Chang, C. C., Fuchs, H., Holland, F., Kita, K., Kondo,
687 Y., Li, X., Lou, S., Shao, M., Zeng, L., Wahner, A., and Zhang, Y.: Amplified trace gas removal in the troposphere,
688 *Science*, 324, 1702-1704, 10.1126/science.1164566, 2009.

689 Hua, W., Chen, Z. M., Jie, C. Y., Kondo, Y., Hofzumahaus, A., Takegawa, N., Chang, C. C., Lu, K. D., Miyazaki,
690 Y., Kita, K., Wang, H. L., Zhang, Y. H., and Hu, M.: Atmospheric hydrogen peroxide and organic hydroperoxides
691 during PRIDE-PRD'06, China: their concentration, formation mechanism and contribution to secondary aerosols,
692 *Atmos. Chem. Phys.*, 8, 6755-6773, 10.5194/acp-8-6755-2008, 2008.

693 Huang, G., Zhou, X., Deng, G., Qiao, H., and Civerolo, K.: Measurements of atmospheric nitrous acid and nitric
694 acid, *Atmos. Environ.*, 36, 2225-2235, [https://doi.org/10.1016/S1352-2310\(02\)00170-X](https://doi.org/10.1016/S1352-2310(02)00170-X), 2002.

695 Huang, R.-J., Yang, L., Cao, J., Wang, Q., Tie, X., Ho, K.-F., Shen, Z., Zhang, R., Li, G., Zhu, C., Zhang, N., Dai,
696 W., Zhou, J., Liu, S., Chen, Y., Chen, J., and O'Dowd, C. D.: Concentration and sources of atmospheric nitrous acid
697 (HONO) at an urban site in Western China, *Sci. Total Environ.*, 593-594, 165-172,
698 <https://doi.org/10.1016/j.scitotenv.2017.02.166>, 2017.

699 Jenkin, M. E., Saunders, S. M., and Pilling, M. J.: The tropospheric degradation of volatile organic compounds: a
700 protocol for mechanism development, *Atmos. Environ.*, 31, 81-104, [http://dx.doi.org/10.1016/S1352-](http://dx.doi.org/10.1016/S1352-2310(96)00105-7)
701 [2310\(96\)00105-7](http://dx.doi.org/10.1016/S1352-2310(96)00105-7), 1997.

702 Jenkin, M. E., Wyche, K. P., Evans, C. J., Carr, T., Monks, P. S., Alfarra, M. R., Barley, M. H., McFiggans, G. B.,
703 Young, J. C., and Rickard, A. R.: Development and chamber evaluation of the MCM v3.2 degradation scheme for
704 β -caryophyllene, *Atmos. Chem. Phys.*, 12, 5275-5308, 10.5194/acp-12-5275-2012, 2012.

705 Kirchstetter, T. W., Harley, A. R., and Littlejohn, D.: Measurement of nitrous acid in motor vehicle exhaust, *Environ.*
706 *Sci. Technol.*, 30, 2843-2849, 10.1021/es960135y, 1996.

707 Kleffmann, J., Becker, K. H., and Wiesen, P.: Heterogeneous NO₂ conversion processes on acid surfaces: possible
708 atmospheric implications, *Atmos. Environ.*, 32, 2721-2729, [https://doi.org/10.1016/S1352-2310\(98\)00065-X](https://doi.org/10.1016/S1352-2310(98)00065-X),
709 1998.

710 Kleffmann, J., Kurtenbach, R., Lörzer, J., Wiesen, P., Kalthoff, N., Vogel, B., and Vogel, H.: Measured and
711 simulated vertical profiles of nitrous acid-Part I: Field measurements, *Atmos. Environ.*, 37, 2949-2955,
712 10.1016/s1352-2310(03)00242-5, 2003.

713 Kleffmann, J., Gavriloaiei, T., Hofzumahaus, A., Holland, F., Koppmann, R., Rupp, L., Schlosser, E., Siese, M.,
714 and Wahner, A.: Daytime formation of nitrous acid: A major source of OH radicals in a forest, *Geophys. Res. Letts.*,
715 32, L05818, 10.1029/2005GL022524, 2005.

716 Kleffmann, J., Lörzer, J. C., Wiesen, P., Kern, C., Trick, S., Volkamer, R., Rodenas, M., and Wirtz, K.:
717 Intercomparison of the DOAS and LOPAP techniques for the detection of nitrous acid (HONO), *Atmos. Environ.*,
718 40, 3640-3652, <https://doi.org/10.1016/j.atmosenv.2006.03.027>, 2006.

719 Kleffmann, J., and Wiesen, P.: Technical Note: Quantification of interferences of wet chemical HONO LOPAP
720 measurements under simulated polar conditions, *Atmos. Chem. Phys.*, 8, 6813-6822, [https://doi.org/10.5194/acp-](https://doi.org/10.5194/acp-8-6813-2008)
721 [8-6813-2008](https://doi.org/10.5194/acp-8-6813-2008), 2008.

722 Kurtenbach, R., Becker, K. H., Gomes, J. A. G., Kleffmann, J., Lörzer, J. C., Spittler, M., Wiesen, P., Ackermann,
723 R., Geyer, A., and Platt, U.: Investigations of emissions and heterogeneous formation of HONO in a road traffic
724 tunnel, *Atmos. Environ.*, 35, 3385-3394, [https://doi.org/10.1016/S1352-2310\(01\)00138-8](https://doi.org/10.1016/S1352-2310(01)00138-8), 2001.

725 Lee, J. D., Whalley, L. K., Heard, D. E., Stone, D., Dunmore, R. E., Hamilton, J. F., Young, D. E., Allan, J. D.,
726 Laufs, S., and Kleffmann, J.: Detailed budget analysis of HONO in central London reveals a missing daytime
727 source, *Atmos. Chem. Phys.*, 16, 2747-2764, 10.5194/acp-16-2747-2016, 2016.

728 Li, G., Lei, W., Zavala, M., Volkamer, R., Dusanter, S., Stevens, P., and Molina, L. T.: Impacts of HONO sources
729 on the photochemistry in Mexico City during the MCMA-2006/MILAGO Campaign, *Atmos. Chem. Phys.*, 10,
730 6551-6567, 10.5194/acp-10-6551-2010, 2010.

731 Li, X., Brauers, T., Haseler, R., Bohn, B., Fuchs, H., Hofzumahaus, A., Holland, F., Lou, S., Lu, K. D., Rohrer, F.,
732 Hu, M., Zeng, L. M., Zhang, Y. H., Garland, R. M., Su, H., Nowak, A., Wiedensohler, A., Takegawa, N., Shao, M.,
733 and Wahner, A.: Exploring the atmospheric chemistry of nitrous acid (HONO) at a rural site in Southern China,
734 *Atmos. Chem. Phys.*, 12, 1497-1513, 10.5194/acp-12-1497-2012, 2012.

735 Liang, Y., Zha, Q., Wang, W., Cui, L., Lui, K. H., Ho, K. F., Wang, Z., Lee, S.-c., and Wang, T.: Revisiting nitrous
736 acid (HONO) emission from on-road vehicles: A tunnel study with a mixed fleet, *J. Air Waste Manage.*, 67, 797-
737 805, 10.1080/10962247.2017.1293573, 2017.

738 Lu, K. D., Rohrer, F., Holland, F., Fuchs, H., Bohn, B., Brauers, T., Chang, C. C., Häsel, R., Hu, M., Kita, K.,
739 Kondo, Y., Li, X., Lou, S. R., Nehr, S., Shao, M., Zeng, L. M., Wahner, A., Zhang, Y. H., and Hofzumahaus, A.:
740 Observation and modelling of OH and HO₂ concentrations in the Pearl River Delta 2006: a missing OH source in
741 a VOC rich atmosphere, *Atmos. Chem. Phys.*, 12, 1541-1569, 10.5194/acp-12-1541-2012, 2012.

742 Ma, Y., Diao, Y., Zhang, B., Wang, W., Ren, X., Yang, D., Wang, M., Shi, X., and Zheng, J.: Detection of
743 formaldehyde emissions from an industrial zone in the Yangtze River Delta region of China using a proton transfer
744 reaction ion-drift chemical ionization mass spectrometer, *Atmos. Meas. Tech.*, 9, 6101-6116, 10.5194/amt-9-6101-
745 2016, 2016.

746 Makkonen, U., Virkkula, A., Mäntykenttä, J., Hakola, H., Keronen, P., Vakkari, V., and Aalto, P. P.: Semi-
747 continuous gas and inorganic aerosol measurements at a Finnish urban site: comparisons with filters, nitrogen in
748 aerosol and gas phases, and aerosol acidity, *Atmospheric Chemistry and Physics*, 12, 5617-5631, 10.5194/acp-12-
749 5617-2012, 2012.

750 Michoud, V., Colomb, A., Borbon, A., Miet, K., Beekmann, M., Camredon, M., Aumont, B., Perrier, S., Zapf, P.,
751 Siour, G., Ait-Helal, W., Afif, C., Kukui, A., Furger, M., Dupont, J. C., Haefelin, M., and Doussin, J. F.: Study of
752 the unknown HONO daytime source at a European suburban site during the MEGAPOLI summer and winter field
753 campaigns, *Atmospheric Chemistry and Physics*, 14, 2805-2822, 10.5194/acp-14-2805-2014, 2014.

754 Monge, M. E., D'Anna, B., Mazri, L., Giroir-Fendler, A., Ammann, M., Donaldson, D. J., and George, C.: Light
755 changes the atmospheric reactivity of soot, *Proc. Natl. Acad. Sci. USA*, 107, 6605-6609, 10.1073/pnas.0908341107,
756 2010.

757 Müller, M., Anderson, B. E., Beyersdorf, A. J., Crawford, J. H., Diskin, G. S., Eichler, P., Fried, A., Keutsch, F. N.,
758 Mikoviny, T., Thornhill, K. L., Walega, J. G., Weinheimer, A. J., Yang, M., Yokelson, R. J., and Wisthaler, A.: In
759 situ measurements and modeling of reactive trace gases in a small biomass burning plume, *Atmos. Chem. Phys.*,
760 16, 3813-3824, 10.5194/acp-16-3813-2016, 2016.

761 Nakashima, Y., and Kajii, Y.: Determination of nitrous acid emission factors from a gasoline vehicle using a chassis
762 dynamometer combined with incoherent broadband cavity-enhanced absorption spectroscopy, *Sci. Total Environ.*,
763 575, 287-293, <https://doi.org/10.1016/j.scitotenv.2016.10.050>, 2017.

764 Nash, T.: Nitrous acid in the atmosphere and laboratory experiments on its photolysis, *Tellus*, 26, 175-179,
765 10.3402/tellusa.v26i1-2.9768, 1974.

766 Ndour, M., D'Anna, B., George, C., Ka, O., Balkanski, Y., Kleffmann, J., Stemmler, K., and Ammann, M.:
767 Photoenhanced uptake of NO₂ on mineral dust: Laboratory experiments and model simulations, *Geophys. Res.*
768 *Letts.*, 35, L05812, 10.1029/2007gl032006, 2008.

769 Neftel, A., Blatter, A., Hesterberg, R., and Staffelbach, T.: Measurements of concentration gradients of HNO₂ and
770 HNO₃ over a semi-natural ecosystem *Atmos. Environ.*, 30 (17), 3017-3025, 1996.

771 Neuman, J. A., Trainer, M., Brown, S. S., Min, K.-E., Nowak, J. B., Parrish, D. D., Peischl, J., Pollack, I. B.,
772 Roberts, J. M., Ryerson, T. B., and Veres, P. R.: HONO emission and production determined from airborne
773 measurements over the Southeast U.S., *J. Geophys. Res. Atmos.*, 121, 9237-9250, 10.1002/2016JD025197, 2016.

774 Nie, W., Ding, A. J., Xie, Y. N., Xu, Z., Mao, H., Kerminen, V. M., Zheng, L. F., Qi, X. M., Huang, X., Yang, X.
775 Q., Sun, J. N., Herrmann, E., Petaja, T., Kulmala, M., and Fu, C. B.: Influence of biomass burning plumes on
776 HONO chemistry in eastern China, *Atmos. Chem. Phys.*, 15, 1147-1159, 10.5194/acp-15-1147-2015, 2015.

777 Perner, D., and Platt, U.: Detection of nitrous-acid in the atmosphere by differential optical-absorption, *Geophys.*
778 *Res. Letts.*, 6, 917-920, 10.1029/GL006i012p00917, 1979.

779 Pinto, J. P., Dibb, J., Lee, B. H., Rappenglück, B., Wood, E. C., Levy, M., Zhang, R. Y., Lefer, B., Ren, X. R., Stutz,
780 J., Tsai, C., Ackermann, L., Golovko, J., Herndon, S. C., Oakes, M., Meng, Q. Y., Munger, J. W., Zahniser, M., and
781 Zheng, J.: Intercomparison of field measurements of nitrous acid (HONO) during the SHARP campaign, *J.*
782 *Geophys. Res. Atmos.*, 119, 5583-5601, 10.1002/2013JD020287, 2014.

783 Platt, U., Perner, D., Harris, G. W., Winer, A. M., and Pitts Jr, J. N.: Observations of nitrous acid in an urban
784 atmosphere by differential optical absorption, *Nature*, 285, 312, 10.1038/285312a0, 1980.

785 Qin, M., Xie, P., Su, H., Gu, J., Peng, F., Li, S., Zeng, L., Liu, J., Liu, W., and Zhang, Y.: An observational study of
786 the HONO-NO₂ coupling at an urban site in Guangzhou City, South China, *Atmos. Environ.*, 43, 5731-5742,
787 <https://doi.org/10.1016/j.atmosenv.2009.08.017>, 2009.

788 Rairoux, P., Koch, B., Moller, D., Göritz, G., Warmbier, G., and Czyzewski, A.: Atmospheric traces monitoring
789 applying Cavity Ring-Down Spectroscopy, *Environ. Sci. Pollut. Res.*, Special issue 4, 68-71, 2002.

790 Ren, X., Brune, W. H., Mao, J., Mitchell, M. J., Leshner, R. L., Simpas, J. B., Metcalf, A. R., Schwab, J. J., Li, Y.,
791 Demerjian, K. L., Felton, H. D., Boynton, G., Adams, A., Perry, J., He, Y., Zhou, X., and Hou, J.: Behavior of OH
792 and HO₂ in the winter atmosphere in New York City: Observations and model comparison, *Atmos. Environ.*, 40,
793 S252-S263, 10.1016/j.atmosenv.2005.11.073, 2006.

794 Ren, X., Gao, H., Zhou, X., Crouse, J. D., Wennberg, P. O., Browne, E. C., LaFranchi, B. W., Cohen, R. C., McKay,
795 M., Goldstein, A. H., and Mao, J.: Measurement of atmospheric nitrous acid at Blodgett Forest during
796 BEARPEX2007, *Atmos. Chem. Phys.*, 10, 6283-6294, 10.5194/acp-10-6283-2010, 2010.

797 Ren, X. R., Harder, H., Martinez, M., Leshner, R. L., Olliger, A., Simpas, J. B., Brune, W. H., Schwab, J. J., Demerjian,
798 K. L., He, Y., Zhou, X. L., and Gao, H. G.: OH and HO₂ chemistry in the urban atmosphere of New York City,
799 *Atmos. Environ.*, 37, 3639-3651, 10.1016/s1352-2310(03)00459-x, 2003.

800 Ren, Y., Ding, A., Wang, T., Shen, X., Guo, J., Zhang, J., Wang, Y., Xu, P., Wang, X., and Gao, J.: Measurement of
801 gas-phase total peroxides at the summit of Mount Tai in China, *Atmospheric Environment*, 43, 1702-1711,
802 10.1016/j.atmosenv.2008.12.020, 2009.

803 Rickard, A. R., Johnson, D., McGill, C. D., and Marston, G.: OH Yields in the Gas-Phase Reactions of Ozone with
804 Alkenes, *The Journal of Physical Chemistry A*, 103, 7656-7664, 10.1021/jp9916992, 1999.

805 Rondon, A., and Sanhueza, E.: High HONO atmospheric concentrations during vegetation burning in the tropical
806 savannah, *Tellus B: Chem. Phys. Meteor.*, 41, 474-477, 10.3402/tellusb.v41i4.15102, 1989.

807 Salmon, O. E., Shepson, P. B., Ren, X., He, H., Hall, D. L., Dickerson, R. R., Stirm, B. H., Brown, S. S., Fibiger,
808 D. L., McDuffie, E. E., Campos, T. L., Gurney, K. R., and Thornton, J. A.: Top-Down Estimates of NO_x and CO
809 Emissions From Washington, D.C.-Baltimore During the WINTER Campaign, *J. Geophys. Res. Atmos.*, 123,
810 7705–7724, 10.1029/2018jd028539, 2018.

811 Scharko, N. K., Martin, E. T., Losovyj, Y., Peters, D. G., and Raff, J. D.: Evidence for Quinone Redox Chemistry
812 Mediating Daytime and Nighttime NO₂-to-HONO Conversion on Soil Surfaces, *Environ. Sci. Technol.*, 51, 9633-
813 9643, 10.1021/acs.est.7b01363, 2017.

814 Sörgel, M., Trebs, I., Wu, D., and Held, A.: A comparison of measured HONO uptake and release with calculated
815 source strengths in a heterogeneous forest environment, *Atmospheric Chemistry and Physics*, 15, 9237-9251,
816 10.5194/acp-15-9237-2015, 2015.

817 Spataro, F., Ianniello, A., Esposito, G., Allegrini, I., Zhu, T., and Hu, M.: Occurrence of atmospheric nitrous acid
818 in the urban area of Beijing (China), *Sci. Total Environ.*, 447, 210-224,
819 <https://doi.org/10.1016/j.scitotenv.2012.12.065>, 2013.

820 Stemmler, K., Ammann, M., Donders, C., Kleffmann, J., and George, C.: Photosensitized reduction of nitrogen
821 dioxide on humic acid as a source of nitrous acid, *Nature*, 440, 195-198, 10.1038/nature04603, 2006.

822 Stemmler, K., Ndour, M., Elshorbany, Y., Kleffmann, J., D'Anna, B., George, C., Bohn, B., and Ammann, M.: Light
823 induced conversion of nitrogen dioxide into nitrous acid on submicron humic acid aerosol, *Atmos. Chem. Phys.*, 7,
824 4237-4248, 10.5194/acp-7-4237-2007, 2007.

825 Stutz, J., Alicke, B., Ackermann, R., Geyer, A., Wang, S. H., White, A. B., Williams, E. J., Spicer, C. W., and Fast,
826 J. D.: Relative humidity dependence of HONO chemistry in urban areas, *J. Geophys. Res. Atmos.*, 109, D03307,
827 doi:10.1029/2003jd004135, 2004.

828 Su, H., Cheng, Y. F., Shao, M., Gao, D. F., Yu, Z. Y., Zeng, L. M., Slanina, J., Zhang, Y. H., and Wiedensohler, A.:
829 Nitrous acid (HONO) and its daytime sources at a rural site during the 2004 PRIDE-PRD experiment in China, *J.*
830 *Geophys. Res. Atmos.*, 113, D14312, 10.1029/2007JD009060, 2008.

831 Su, H., Cheng, Y., Oswald, R., Behrendt, T., Trebs, I., Meixner, F. X., Andreae, M. O., Cheng, P., Zhang, Y., and
832 Poschl, U.: Soil nitrite as a source of atmospheric HONO and OH radicals, *Science*, 333, 1616-1618,
833 10.1126/science.1207687, 2011.

834 Tang, Y., An, J., Wang, F., Li, Y., Qu, Y., Chen, Y., and Lin, J.: Impacts of an unknown daytime HONO source on
835 the mixing ratio and budget of HONO, and hydroxyl, hydroperoxyl, and organic peroxy radicals, in the coastal
836 regions of China, *Atmos. Chem. Phys.*, 15, 9381-9398, 10.5194/acp-15-9381-2015, 2015.

837 Tanner, D. J., and Eisele, F. L.: Present oh measurement limits and associated uncertainties, *J. Geophys. Res. Atmos.*,
838 100, 2883-2892, 1995.

839 Trick, S.: Formation of nitrous acid on urban surfaces - a physicalchemical perspective, Ph.D. thesis, University of
840 Heidelberg, 2004.

841 Trinh, H. T., Imanishi, K., Morikawa, T., Hagino, H., and Takenaka, N.: Gaseous nitrous acid (HONO) and nitrogen
842 oxides (NO_x) emission from gasoline and diesel vehicles under real-world driving test cycles, *J. Air Waste Manage.*,
843 67, 412-420, 10.1080/10962247.2016.1240726, 2017.

844 VandenBoer, T. C., Brown, S. S., Murphy, J. G., Keene, W. C., Young, C. J., Pszenny, A. A. P., Kim, S., Warneke,
845 C., de Gouw, J. A., Maben, J. R., Wagner, N. L., Riedel, T. P., Thornton, J. A., Wolfe, D. E., Dubé, W. P., Öztürk,
846 F., Brock, C. A., Grossberg, N., Lefter, B., Lerner, B., Middlebrook, A. M., and Roberts, J. M.: Understanding the
847 role of the ground surface in HONO vertical structure: High resolution vertical profiles during NACHTT-11, *J.*
848 *Geophys. Res. Atmos.*, 118, 10,155-110,171, 10.1002/jgrd.50721, 2013.

849 Vecera, Z., and Dasgupta, P. K.: Measurement of ambient nitrous acid and a reliable calibration source for gaseous
850 nitrous acid, *Environ. Sci. Technol.*, 25, 255-260, 10.1021/es00014a006, 1991.

851 Villena, G., Kleffmann, J., Kurtenbach, R., Wiesen, P., Lissi, E., Rubio, M. A., Croxatto, G., and Rappenglück, B.:
852 Vertical gradients of HONO, NO_x and O₃ in Santiago de Chile, *Atmos. Environ.*, 45, 3867-3873,
853 10.1016/j.atmosenv.2011.01.073, 2011.

854 Villena, G., Bejan, I., Kurtenbach, R., Wiesen, P., and Kleffmann, J.: Interferences of commercial NO₂ instruments
855 in the urban atmosphere and in a smog chamber, *Atmos. Meas. Tech.*, 5, 149-159, 10.5194/amt-5-149-2012, 2012.

856 Wall, K. J., and Harris, G. W.: Uptake of nitrogen dioxide (NO₂) on acidic aqueous humic acid (HA) solutions as a
857 missing daytime nitrous acid (HONO) surface source, *J. Atmos. Chem.*, 74, 283-321, 10.1007/s10874-016-9342-
858 8, 2016.

859 Wang, J., Zhang, X., Guo, J., Wang, Z., and Zhang, M.: Observation of nitrous acid (HONO) in Beijing, China:
860 Seasonal variation, nocturnal formation and daytime budget, *Sci. Total Environ.*, 587-588, 350-359,
861 <https://doi.org/10.1016/j.scitotenv.2017.02.159>, 2017.

862 Wang, L., Wen, L., Xu, C., Chen, J., Wang, X., Yang, L., Wang, W., Yang, X., Sui, X., Yao, L., and Zhang, Q.:
863 HONO and its potential source particulate nitrite at an urban site in North China during the cold season, *The Science*
864 *of the total environment*, 538, 93-101, 10.1016/j.scitotenv.2015.08.032, 2015a.

865 Wang, M., Chen, W. T., Shao, M., Lu, S. H., Zeng, L. M., and Hu, M.: Investigation of carbonyl compound sources
866 at a rural site in the Yangtze River Delta region of China, *Journal of Environmental Sciences-China*, 28, 128-136,
867 10.1016/j.jes.2014.12.001, 2015b.

868 Wang, S., Zhou, R., Zhao, H., Wang, Z., Chen, L., and Zhou, B.: Long-term observation of atmospheric nitrous
869 acid (HONO) and its implication to local NO₂ levels in Shanghai, China, *Atmos. Environ.*, 77, 718-724,
870 <https://doi.org/10.1016/j.atmosenv.2013.05.071>, 2013.

871 Wong, K. W., Oh, H. J., Lefer, B. L., Rappenglück, B., and Stutz, J.: Vertical profiles of nitrous acid in the nocturnal
872 urban atmosphere of Houston, TX, *Atmos. Chem. Phys.*, 11, 3595-3609, 10.5194/acp-11-3595-2011, 2011.

873 Wong, K. W., Tsai, C., Lefer, B., Haman, C., Grossberg, N., Brune, W. H., Ren, X., Luke, W., and Stutz, J.: Daytime
874 HONO vertical gradients during SHARP 2009 in Houston, TX, *Atmospheric Chemistry and Physics*, 12, 635-652,
875 10.5194/acp-12-635-2012, 2012.

876 Wong, K. W., Tsai, C., Lefer, B., Grossberg, N., and Stutz, J.: Modeling of daytime HONO vertical gradients during
877 SHARP 2009, *Atmos. Chem. Phys.*, 13, 3587-3601, 10.5194/acp-13-3587-2013, 2013.

878 Xu, Z., Wang, T., Wu, J., Xue, L., Chan, J., Zha, Q., Zhou, S., Louie, P. K. K., and Luk, C. W. Y.: Nitrous acid
879 (HONO) in a polluted subtropical atmosphere: Seasonal variability, direct vehicle emissions and heterogeneous
880 production at ground surface, *Atmos. Environ.*, 106, 100-109, <http://dx.doi.org/10.1016/j.atmosenv.2015.01.061>,
881 2015.

882 Xue, L., Gu, R., Wang, T., Wang, X., Saunders, S., Blake, D., Louie, P. K. K., Luk, C. W. Y., Simpson, I., Xu, Z.,
883 Wang, Z., Gao, Y., Lee, S., Mellouki, A., and Wang, W.: Oxidative capacity and radical chemistry in the polluted
884 atmosphere of Hong Kong and Pearl River Delta region: analysis of a severe photochemical smog episode,
885 *Atmospheric Chemistry and Physics*, 16, 9891-9903, 10.5194/acp-16-9891-2016, 2016.

886 Ye, C., Zhou, X., Pu, D., Stutz, J., Festa, J., Spolaor, M., Tsai, C., Cantrell, C., Mauldin, R. L., Campos, T.,
887 Weinheimer, A., Hornbrook, R. S., Apel, E. C., Guenther, A., Kaser, L., Yuan, B., Karl, T., Haggerty, J., Hall, S.,
888 Ullmann, K., Smith, J. N., Ortega, J., and Knote, C.: Rapid cycling of reactive nitrogen in the marine boundary
889 layer, *Nature*, 532, 489-491, 10.1038/nature17195, 2016.

890 Ye, C., Zhang, N., Gao, H., and Zhou, X.: Photolysis of Particulate Nitrate as a Source of HONO and NO_x, *Environ.*
891 *Sci. Technol.*, 51, 6849-6856, 10.1021/acs.est.7b00387, 2017.

892 Zhang, N., Zhou, X., Shepson, P. B., Gao, H., Alaghmand, M., and Stirm, B.: Aircraft measurement of HONO
893 vertical profiles over a forested region, *Geophys. Res. Letts.*, 36, L15820, 10.1029/2009gl038999, 2009.

894 Zheng, J., Ma, Y., Chen, M., Zhang, Q., Wang, L., Khalizov, A. F., Yao, L., Wang, Z., Wang, X., and Chen, L.:
895 Measurement of atmospheric amines and ammonia using the high resolution time-of-flight chemical ionization
896 mass spectrometry, *Atmos. Environ.*, 102, 249-259, <http://dx.doi.org/10.1016/j.atmosenv.2014.12.002>, 2015a.

897 Zheng, J., Ma, Y., Chen, M., Zhang, Q., Wang, L., Khalizov, A. F., Yao, L., Wang, Z., Wang, X., and Chen, L.:
898 Measurement of atmospheric amines and ammonia using the high resolution time-of-flight chemical ionization
899 mass spectrometry, *Atmospheric Environment*, 102, 249-259, 10.1016/j.atmosenv.2014.12.002, 2015b.

900 Zhou, X., Civerolo, K., Dai, H., Huang, G., Schwab, J., and Demerjian, K.: Summertime nitrous acid chemistry in
901 the atmospheric boundary layer at a rural site in New York State, *J. Geophys. Res. Atmos.*, 107, ACH 13-11-ACH
902 13-11, 10.1029/2001jd001539, 2002.

903 Zhou, X., Gao, H., He, Y., Huang, G., Bertman, S. B., Civerolo, K., and Schwab, J.: Nitric acid photolysis on
904 surfaces in low-NO_x environments: Significant atmospheric implications, *Geophys. Res. Letts.*, 30, 2217,

905 10.1029/2003gl018620, 2003.

906 Zhou, X., Zhang, N., TerAvest, M., Tang, D., Hou, J., Bertman, S., Alaghmand, M., Shepson, P. B., Carroll, M. A.,
907 Griffith, S., Dusanter, S., and Stevens, P. S.: Nitric acid photolysis on forest canopy surface as a source for
908 tropospheric nitrous acid, *Nat. Geosci.*, 4, 440-443, 10.1038/ngeo1164, 2011.

909 Ziemba, L. D., Dibb, J. E., Griffin, R. J., Anderson, C. H., Whitlow, S. I., Lefler, B. L., Rappenglück, B., and Flynn,
910 J.: Heterogeneous conversion of nitric acid to nitrous acid on the surface of primary organic aerosol in an urban
911 atmosphere, *Atmos. Environ.*, 44, 4081-4089, 10.1016/j.atmosenv.2008.12.024, 2010.

912

913

914 **Table 1.** Overview on HONO measurements performed in Nanjing and other cities in China.

Location	Date	HONO (ppbv)[#]	References
Beijing	Sep. - Oct. 2015 (autumn)	2.27 ± 1.82	Wang et al. (2017)
	Jan. 2016 (winter)	1.05 ± 0.89	
	Apr. - May 2016 (spring)	1.05 ± 0.95	
	Jun. - Jul. 2016 (summer)	1.38 ± 0.90	
Xi'an	Jul. - Aug. 2015 (summer)	1.12 ± 0.97	Huang et al. (2017)
Jinan	Nov. 2013 - Jan. 2014 (winter)	0.35 ± 0.5	Wang et al. (2015a)
Nanjing	Apr. - Jun. 2012 (spring)	0.76 ± 0.79	Nie et al. (2015)
Xianghe	Mar 2010 - Dec 2012	0.33 ± 0.16 [*]	Hendrick et al. (2014)
Beijing	Jan. - Feb. 2007(winter)	1.04 ± 0.73	Spataro et al. (2013)
Guangzhou	Jul. 2006 (summer)	0.71~8.43 (2.8) ^{**}	Qin et al. (2009)
Xinken	Oct. - Nov. 2004 (autumn)	0.4~3.8 (1.2) ^{**}	Li et al. (2012)
Nanjing	Dec. 2015 (winter)	1.32 ± 0.92	This work

915 [#]Campaign averaged; ^{*}Yearly average; ^{**}Only range and mean values are reported

916

917 **Table 2.** Ozonolysis reaction rate constants and OH formation yields of the volatile organic compounds (VOC)
 918 used in the calculation.

VOC	$k(298\text{K}) \times 10^{-18}$ ($\text{cm}^3\text{molecule}^{-1}\text{s}^{-1}$) ^a	OH yield	VOC	$k(298\text{K}) \times 10^{-18}$ ($\text{cm}^3\text{molecule}^{-1}\text{s}^{-1}$) ^a	OH yield
Ethene	1.6	0.13 ^b	trans-2-Pentene	160	0.47 ^c
Propene	10.1	0.34 ^b	cis-2-Pentene	130	0.3 ^c
trans-2-Butene	190	0.59 ^b	1-Pentene	10.6	0.37 ^b
cis-2-Butene	125	0.37 ^b	Isoprene	12.8 ^c	0.13 ± 0.03 ^c
1-Butene	9.64	0.41 ^b	Styrene	17	0.07 ^c

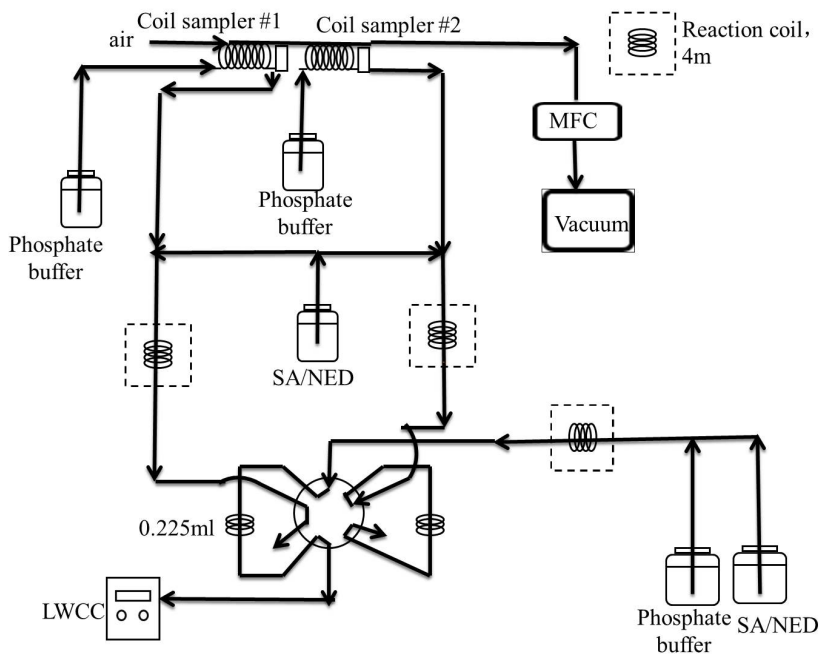
a: Atkinson and Arey (2003); b: Rickard et al. (1999); c: Alicke et al. (2002)

919
 920

921 **Table 3.** Linear correlation coefficients (Pearson correlation, R) of the unknown source to HONO production-
 922 related parameters.

Individual	Correlation Coefficient (R)	Various Combinations of	Correlation Coefficient (R)
RH	<u>0.27</u>	J(NO ₂)-S/V	<u>0.59</u>
NO ₂	<u>0.31</u>	J(NO ₂)-NO ₂	<u>0.51</u>
S/V	<u>0.33</u>	J(NO ₂)-RH	<u>0.59</u>
J(NO ₂)	<u>0.31</u>	J(NO ₂)-NO ₂ -RH	<u>0.70</u>
NO ₂ -S/V	<u>0.36</u>	J(NO ₂)-NO ₂ -S/V	<u>0.61</u>
NO ₂ -RH	<u>0.40</u>	NO ₂ -RH-S/V	<u>0.44</u>
RH-S/V	<u>0.39</u>	J(NO ₂)-NO ₂ -S/V-RH	<u>0.70</u>

923
 924

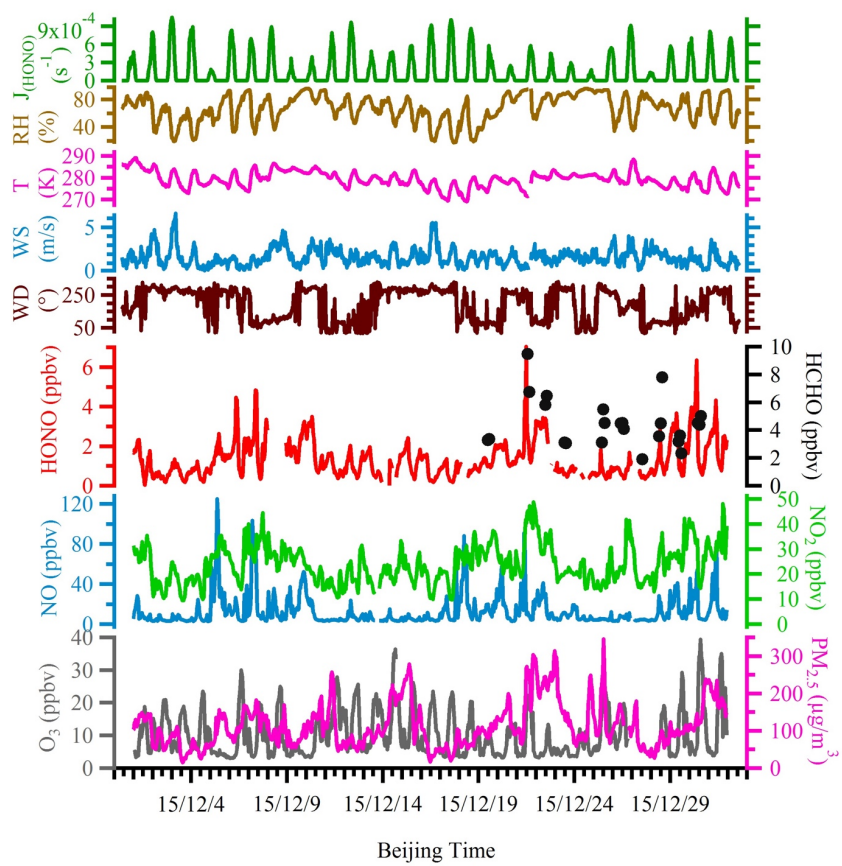


925

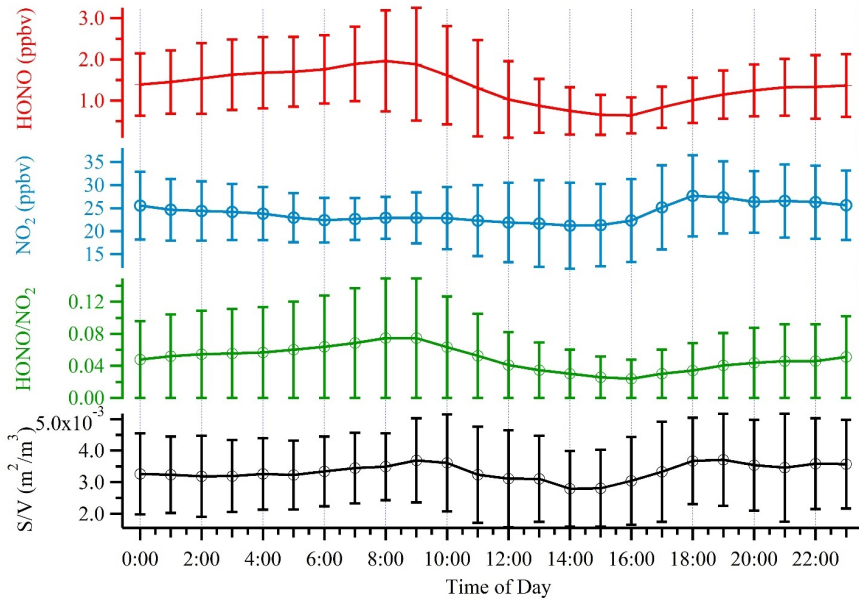
926

Figure 1. Schematics of the custom-built wet chemistry-based HONO instrument.

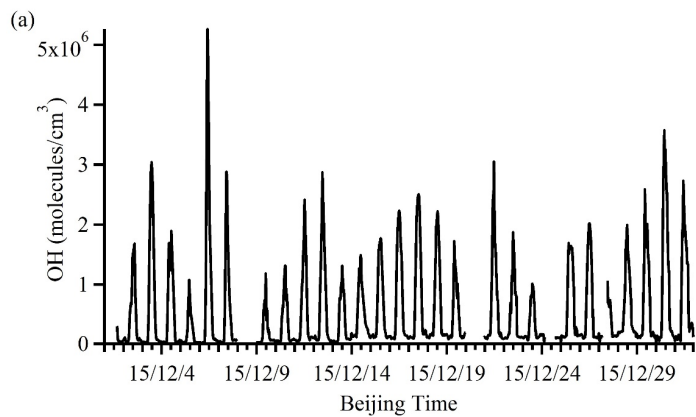
927



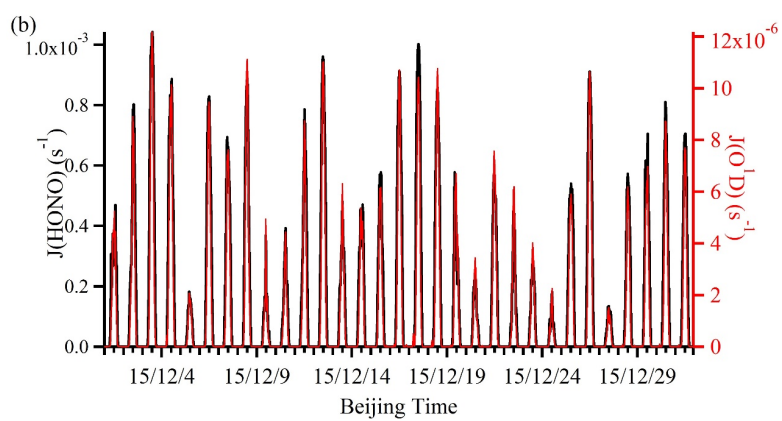
928
 929 **Figure 2.** Time series of meteorological parameters, including HONO photolysis frequency (J(HONO)), relative
 930 humidity (RH), ambient temperature, wind speed and wind direction, as well as mixing ratios of measured HONO,
 931 HCHO, NO, NO₂, O₃ and PM_{2.5} during the observation period.
 932



934
 935 **Figure 3.** Average diurnal profiles of HONO, NO₂, HONO/NO₂ and S/V. Error bars represent the standard
 936 deviations in hourly bins.



938

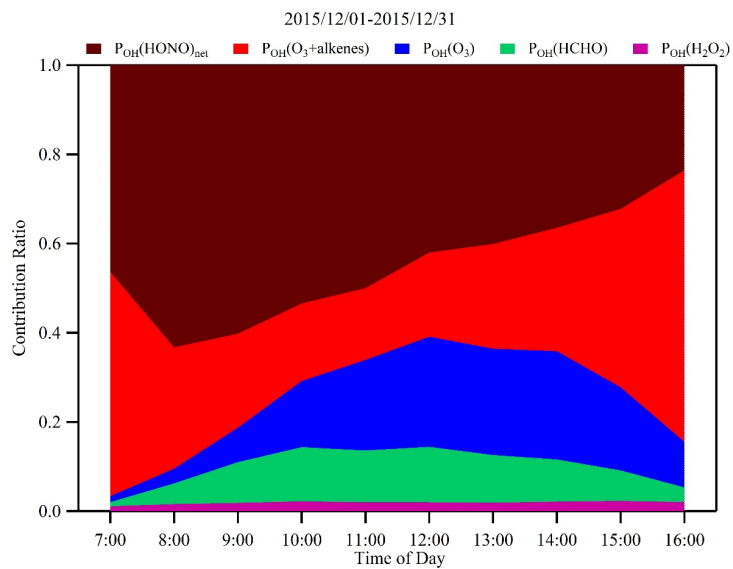


939

940 **Figure 4.** Time series of simulated OH (panel a) and observed photolysis rates (J(HONO) and J(O¹D)) (panel b).

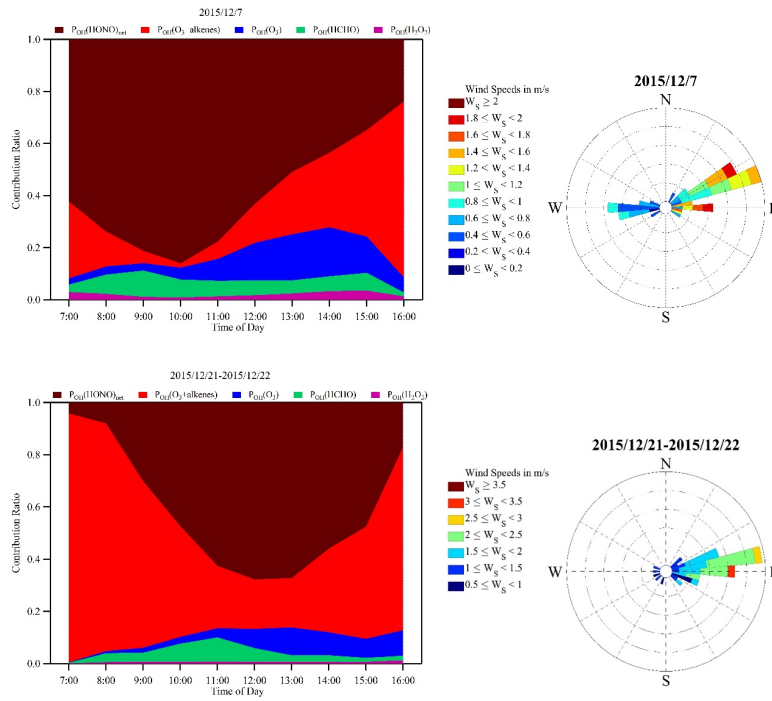
941 The gaps in the OH time series were the time periods when some observation data were not available.

942



943
 944 **Figure 5.** Campaign averaged diurnal variations of contribution fractions of OH production rates from HONO
 945 photolysis (brown), alkene ozonolysis (red), O₃ photolysis (blue), HCHO photolysis (green), and H₂O₂ photolysis
 946 (purple).
 947

948



949

950

951

952 **Figure 6.** The same plots as Fig. 5 during two industrial plume events on the 7th (upper panel) and from the 21st-

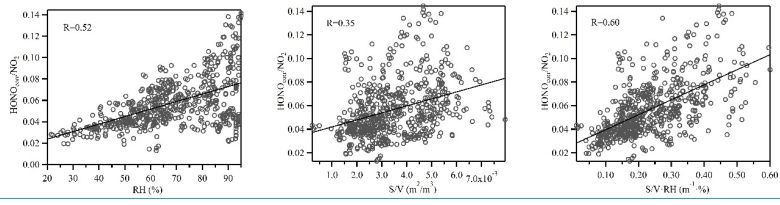
953 22nd (lower panel) of December 2015. The corresponding wind rose plots indicate the origin of these plumes, i.e.,

954 the industry park to the east of the observation site.

955

956

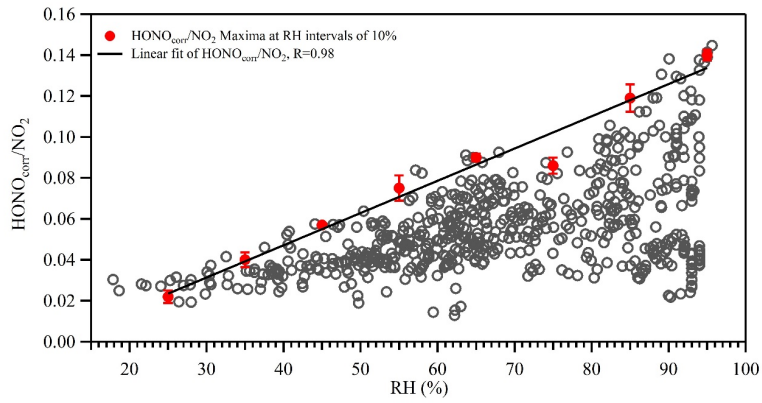
957



958

Figure 7. Nighttime correlations between HONO/NO₂ and RH, S/V and the product of S/V·RH.

959



960

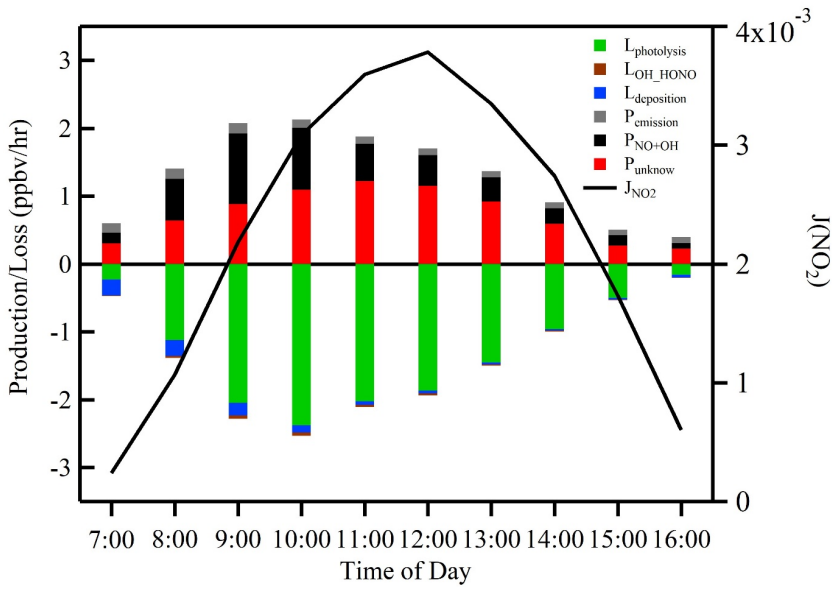
961 **Figure 8.** Correlation between HONO/NO₂ and relative humidity (RH) at night. The open gray circles are 30-min

962 averages. The red circles represent the averages of the top-5 maxima of HONO/NO₂ ratios in 10% RH bins. Error

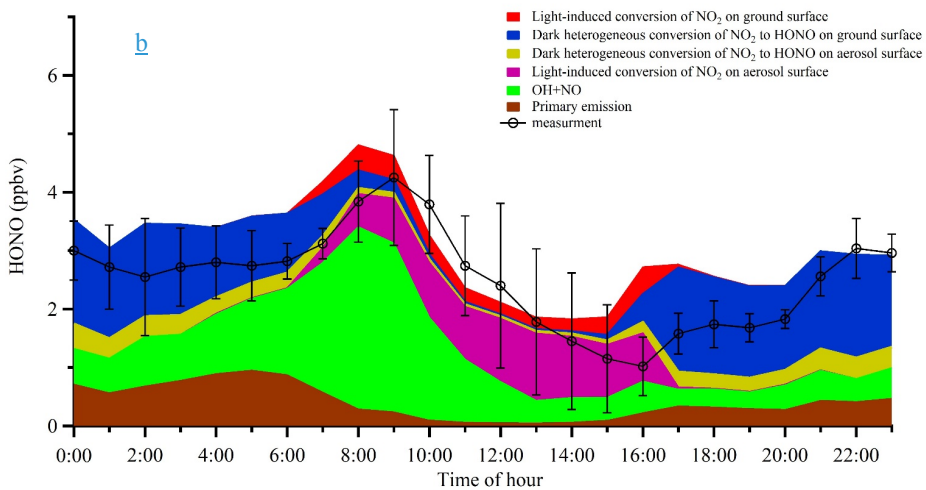
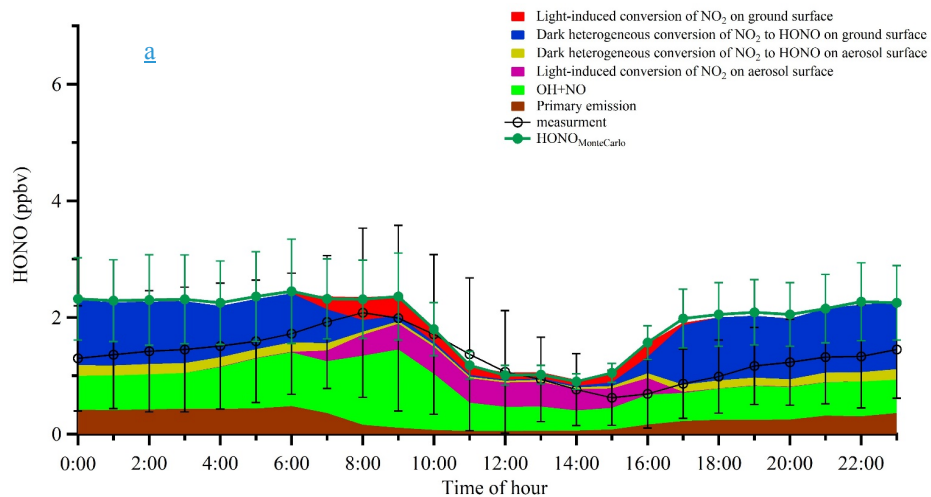
963 bars represent standard deviations of the top-5 HONO/NO₂ ratios in 10% RH bins. The black line is the linear fit

964 of the red circles for HONO/NO₂ with RH.

965



966
 967 **Figure 9.** Averaged production and loss rates of daytime HONO and J(NO₂) during the measurement period. The
 968 black line shows the photolysis rate of NO₂.



969 **Figure 10.** a) [Averaged diurnal profiles of the measured HONO and the modeled HONO from different sources.](#)
 970 [Error bars on the black line represent standard deviations of HONO measurements in hourly bins. Error bars on the](#)
 971 [green markers denote the Monte Carlo analysis results;](#) b) The same plot as panel a, except that only the two
 972 industrial plume events (the 7th and from the 21st to 22nd [of December 2015](#)) were considered in the model.

973